Colossal magnetoresistance

1997 J. Phys.: Condens. Matter 9 8171

(http://iopscience.iop.org/0953-8984/9/39/005)

J. Phys.: Condens. Matter **9** (1997) 8171–8199. Printed in the UK PII: S0953-8984(97)72445-7

REVIEW ARTICLE

Colossal magnetoresistance

A P Ramirez

Bell Laboratories, Lucent Technologies, 600 Mountain Avenue, Murray Hill, NJ 07974-0636, USA

Received 1 July 1997

Abstract. We review recent experimental work falling under the broad classification of colossal magnetoresistance (CMR), which is magnetoresistance associated with a ferromagnetic-to-paramagnetic phase transition. The prototypical CMR compound is derived from the parent compound, perovskite $LaMnO_3$. When hole doped at a concentration of 20–40% holes/Mn ion, for instance by Ca or Sr substitution for La, the material displays a transition from a high-temperature paramagnetic insulator to a low-temperature ferromagnetic metal. Near the phase transition temperature, which can exceed room temperature in some compositions, large magnetoresistance is observed and its possible application in magnetic recording has revived interest in these materials. In addition, unusual magneto-elastic effects and charge ordering have focused attention on strong electron–phonon coupling. This coupling, which is a type of dynamic extended-system version of the Jahn–Teller effect, in conjunction with the double-exchange interaction, is also viewed as essential for a microscopic description of CMR in the manganite perovskites. Large magnetoresistance is also seen in other systems, namely $Tl_2Mn_2O_7$ and some Cr chalcogenide spinels, compounds which differ greatly from the manganite perovskites. We describe the relevant points of contrast between the various CMR materials.

1. Introduction

During the last decade, interest has grown in heterogeneous ferromagnetic materials, such as thin-film multilayers and cluster-alloy compounds which display so-called giant magnetoresistance (GMR). The interest in these systems stems from the prospect of their use in magnetic recording—indeed, prototype disk drives employing GMR read heads present a challenge to traditional MR read-head technology [1]. More recently, it has become recognized that some materials, specifically 3d transition-metal oxides, possess large room-temperature magnetoresistivity associated with a paramagnetic–ferromagnetic phase transition. The growth of interest in their properties stems in large part from the prospect of creating metal oxide devices whose performance exceeds GMR devices. In addition, it is now recognized that the large magnetoresistivity in these oxides is the result of a unique type of metal–insulator transition, the understanding of which complements the drive for applications.

The compounds which have been the focus of the majority of studies are the manganite perovskites $T_{1-x}D_xMnO_3$ where T is a trivalent lanthanide cation (e.g. La) and D is a divalent, e.g. alkaline-earth (e.g. Ca, Sr, Ba), cation. For the end members of the dilution series, $LaMnO_3$ and $CaMnO_3$, the ground state is antiferromagnetic (AF), as expected for spins interacting via the superexchange interaction when the metal–oxygen–metal bond angle is close to 180° [2]. In a certain range of doping, $x \approx 0.2$–0.4, the ground state is ferromagnetic (FM), and the paramagnetic-to-ferromagnetic transition is accompanied

0953-8984/97/398171+29$19.50

by a sharp drop in resistivity $\rho(T)$. This phenomenon has been known to exist since 1950 [3, 4]. Recently, interest in these materials has been renewed by the realization that (i) the magnetoresistance (MR) associated with this correlation between magnetization (M) and resistivity (ρ) can be very large, and (ii) the basic interaction responsible for the ρ–M correlation, the double-exchange (DE) interaction [5–7] between heterovalent (Mn^{3+}, Mn^{4+}) neighbours, is by itself not sufficient to explain this MR [8]. Both the large resistance and the associated MR are now thought to be related to the formation of small lattice polarons in the paramagnetic state. The large MR resulting from the transition has been called 'colossal magnetoresistance' [9], mainly to distinguish it as a phenomenon distinct from GMR. In addition to the renewed interest in the FM state, much attention has been given to another type of collective state, charge order (CO), typically observed for $x > 0.3$. At these doping levels CO can compete with the FM ground state, leading to complex electronic phase behaviour as chemical formula is varied [10–12]. Perhaps the biggest intellectual advance in understanding these disparate effects is the realization of the importance of electron–phonon (e–ph) coupling. Several theories have elucidated the role of e–ph coupling in producing CMR [13, 14]. It is also widely held that this e–ph coupling is necessary to explain not only CMR, but also (i) the polaron signatures in transport studies (see section 3), (ii) the large isotope effect on the FM Curie temperature [15], (iii) the large Debye–Waller factors [16] and (iv) the CO state and its large sound velocity anomalies [12]. The microscopic origin of strong e–ph coupling is the large Jahn–Teller effect which occurs for d^4 ions in an octahedral ligand environment [17]. For the undoped material ($x = 0$) this results in a large static structural distortion [18]. The question of how this e–ph coupling manifests itself in the CMR range ($x \approx 0.2$–0.4) is one of the central questions to be addressed by theory.

The understanding developed to explain CMR in the manganite perovskites does not carry over easily to two other CMR compound families—the pyrochlores, e.g. $Tl_2Mn_2O_7$ [19], and the spinels ACr_2Ch_4 where A = Fe, Cu, Cd (for example) is a tetrahedrally coordinated cation and Ch is a chalcogen (S, Se, Te) [20]. Like the manganese perovskites, these compounds exhibit large drops in resistivity at their FM T_C values. However, unlike the perovskites, they possess (i) no mixed valency (and as a result, have low carrier density), (ii) an A-site cation (Tl or A) capable of contributing states at the Fermi level, and (iii) large deviations of the metal–anion–metal bond angle from 180°.

In this review, we collect some experimental results necessary for an empirical understanding of the various ground states in the manganite perovskites and present a comparison between the different compounds exhibiting CMR. Since the field is large and rapidly developing, there are sure to be oversights among the citations, and for these we apologize in advance.

2. Materials

2.1. Structure and electronic spectrum

Jonker and van Santen synthesized and characterized [3] a series of compounds with the general formula $T_{1-x}D_xMnO_3$ where T is a trivalent ion and D is a divalent ion. These compounds form in the structure of perovskite, $CaTiO_3$. In this structure, the T, D and M ions form interpenetrating simple cubic sublattices with O at the cube faces and edges, as shown schematically to the right in figure 1. The crystal structure and lattice parameters obtained by neutron powder diffraction are given by Elemans *et al* for a series of solid solutions $La_{1-x}Ba_xMn_{1-y}Ti_yO_3$ [18]. All the compounds studied, which include the end member $LaMnO_3$, are isostructural, crystallizing in the orthorhombic *Pnma* structure at

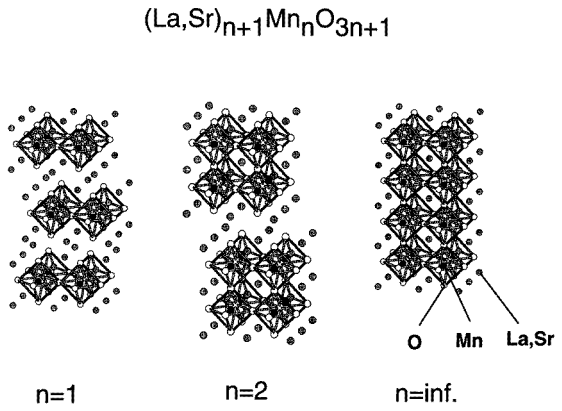

Figure 1. Schematic structures of the Ruddelsden–Popper series of layered compounds. Here n is the number of connected layers of vertex-sharing MnO_6 octahedra. For $n = 1$, the structure is that of K_2NiF_4 and $n = 2$ is the bilayer structure (both have tetragonal space groups $I4/mmm$, $Z = 2$), and $n = \infty$ the distorted perovskite structure (rhombohedral space group ($R\bar{3}c$;$Z = 2$)). The room-temperature lattice parameters are $a = b = 3.86(1)$ Å and $c = 12.48(8)$ Å for $n = 1$; $a = b = 3.87(9)$ Å and $c = 20.14(4)$ Å for $n = 2$; $a = 5.45(8)$ Å for $n = \infty$. (Reproduced from [58]).

room temperature. The end member $LaMnO_3$ is very distorted: the octahedra are elongated and tilted. Though tilting distortions are not unusual for perovskites simply on the basis of steric conditions, its magnitude in $LaMnO_3$ and the presence of elongation are thought to be the result of a Jahn–Teller local distortion [18, 21]. Jirak *et al* have shown that for $Pr_{1-x}Ca_xMnO_3$, there exists a phase transition between a high-temperature pseudo-cubic phase and an orthorhombic phase [22]. This structural transition temperature exceeds 900 K for $x = 0$ and decreases to room temperature at around $x = 0.3$, the doping level where the FM state appears, suggesting a strong magneto-elastic coupling. The structure of compounds exhibiting CMR is usually orthorhombic but, as described below in section 2.2, for doping levels near the $T = 0$ metal–insulator boundary, the symmetry can be modified by application of magnetic field.

The early work of Jonker and van Santen established the range of possible solid solutions allowed by the Goldschmidt tolerance factor $t = (r_D + r_O)/\sqrt{2}(r_T + r_O) \approx 1$, where r_D, r_T, and r_O are the radii of the divalent, trivalent, and oxygen ions, respectively [3]. The tolerance factor measures the deviation from perfect cubic structure ($t = 1$). By using mixtures of T = La, Pr, and Nd and D = Ca, Sr, Ba, and Pb, t can be varied, with the result that the perovskite structure is stable for $0.85 < t < 0.91$. At finite doping, charge balance is maintained by a fraction, x, of Mn ions assuming a tetravalent, Mn^{4+} (d^3), configuration in a random fashion throughout the crystal, with the remainder in the Mn^{3+} (d^4) state. Presumably, D substitution is equivalent to hole doping, but thermopower and Hall effect disagree on the carrier sign in the paramagnetic state, suggesting that a simple band picture is not valid (see section 3.1). Mixed valency can also be modified by varying the oxygen content. For $x \approx 0$ and 1, $M(T < 100$ K) was found to be small, indicating an antiferromagnetic (AF) ground state. At intermediate values of x, M rises and peaks with its Hund's-rule value at $x \approx 0.3$. In subsequent work [4] van Santen and Jonker showed that at temperatures above the ferromagnetic Curie point, T_C, the resistivity behaves like a semiconductor, $d\rho/dT < 0$, but that below T_C, not only is there a sharp reduction in

resistivity, but also a transition to metallic behaviour, $d\rho/dT > 0$. This behaviour is shown for $La_{1-x}Sr_xMnO_3$ and $La_{1-x}Ca_xMnO_3$ in figures 2 and 3.

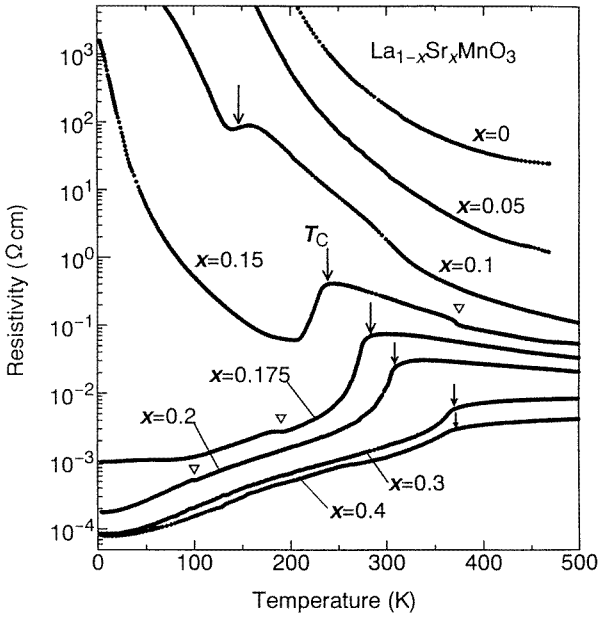

Figure 2. Resistivity against T for $La_{1-x}Sr_xMnO_3$ for various x values. The arrows denote the transition as determined by magnetization measurements. (Reproduced from [33].)

Zener proposed a mechanism he called 'double exchange' (DE) to explain the simultaneous occurrence of ferromagnetism and metallicity, both as a function of x and T, found by Jonker and van Santen [5]. The FM state is observed only for finite D concentration where electronic transport is via holes arising from charge exchange between Ca^{2+}, for example, and Mn. For $x < 0.5$ the majority of Mn ions are in the d^4 configuration which, for octahedral coordination, means a half-filled t_{2g} triplet and a quarter-filled e_g doublet. The minority of sites are d^3 which corresponds to a half-filled t_{2g} orbital triplet. Hund's rule dictates that as the hole hops from site to site, it is accompanied by a reduction in S from 2 to 3/2 (Hund's energy $J_H \gg t$, the transfer integral). This hopping is impeded if neighbouring sites are orthogonal, i.e. spins not parallel. Anderson and Hasegawa showed that the transfer integral varies as the cosine of the angle between neighbouring spins [6]. As temperature is lowered and spin fluctuations decrease, the combined itinerant/local-moment system lowers its total energy by aligning the spins ferromagnetically and allowing the itinerant electrons to gain kinetic energy. Recently, Millis *et al* have shown that a Hamiltonian incorporating only the DE interaction cannot explain the most obvious feature of the manganites, namely the magnitude of the change in resistivity at the FM transition [8]. They, as well as Röder *et al*, proposed, in addition to DE, an electron–phonon coupling term [13, 14]. Such an interaction is not unexpected in a picture where transport is via hopping among Mn^{3+} and Mn^{4+} ions. Here, the hole, corresponding to an Mn^{4+} (d^3) ion must displace a Mn^{3+} (d^4) ion which, in the dilute limit, can be associated with a large Jahn–Teller (J–T) coupling. An analysis of acoustic resonance experiments for dilute Cr^{2+} in MgO shows that the O^{2-} ions are displaced by roughly 1.5 Å from their undistorted positions [17]. Here, Cr^{2+} is, like Mn^{3+} in $LaMnO_3$, a d^4 ion in an octahedral oxygen environment. This distortion is

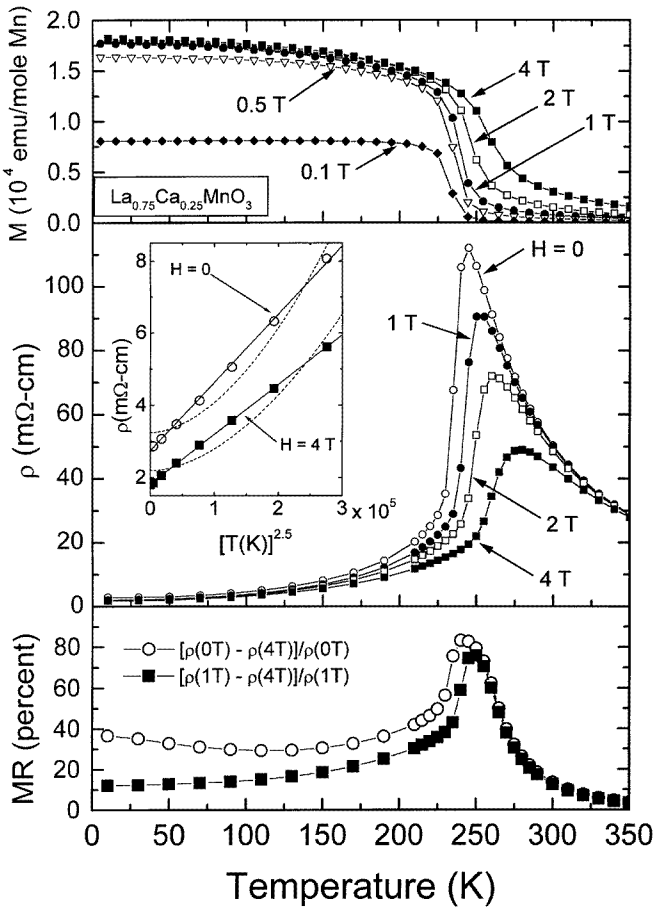

Figure 3. Top frame: magnetization against temperature for $La_{0.75}Ca_{0.25}MnO_3$ for various field values. Middle frame: resistivity against temperature. The inset shows the low-temperature resistivity compared to $T^{2.5}$ (solid line) and $T^{4.5}$ (dashed line) behaviour. Bottom frame: magnetoresistance against temperature. Open symbols reflect low-field behaviour and solid symbols reflect the high-field behaviour. (Reproduced from [42].)

of similar magnitude as that in $LaMnO_3$ and, most likely, arises from the manifestation of the strong electron–phonon coupling implied by the J–T theorem in the dilute case. Even though the J–T theorem applies strictly only for single ions, the large distortion found in the acoustic resonance experiments suggests an e–ph coupling of a size which must also play a significant role for interacting ions. Using a different approach, Varma has attributed the main CMR effect to reduction of localization by spin fluctuation scattering with the application of a magnetic field [23].

The picture just outlined, of electronic hopping within narrow and fully spin-polarized bands is supported by a band structure calculation made for the end members of one dilution series, $LaMnO_3$ and $CaMnO_3$ [24]. For $LaMnO_3$ this calculation shows a typical separation between up- and down-polarized bands of about 1.5 eV and band widths of order 1–1.5 eV. Photoemission experiments on $La_{1-x}D_xMnO_3$ (D = Ca, Pb) confirm these basic features [25]. The density of states for such a system is shown schematically in figure 4. Also

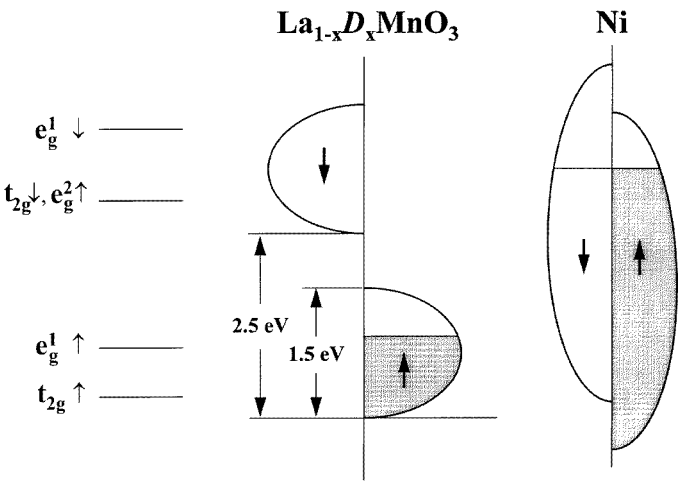

Figure 4. Schematic $T = 0$ density of states for doped $LaMnO_3$. The level diagram to the left shows the approximate positions of the 3d bands in undoped $LaMnO_3$, from [24]. The energy scale for $La_{2/3}Sr_{1/3}MnO_3$ is extracted from photoemission data [25]. Comparison is made to Ni metal which possesses a much smaller degree of spin polarization. (Figure adapted from [104].)

shown for comparison is the density of states for Ni metal. Since the up- and down-spin bands are well separated, the magnetic polarization (saturation moment) is 100%, compared to 11% in Ni. This will lead to reversal of carrier spin direction across FM domains, and large grain-boundary effects as detailed in section 3.2.

2.2. Comparison to GMR

The recent renewal of interest started with the work of Kusters *et al* [26] on $Nd_{0.5}Pb_{0.5}MnO_3$, and Jirak *et al* [22] on $Pr_{1-x}Ca_xMnO_3$. More recently, thin films were studied by von Helmolt *et al* ($La_{0.67}Ba_{0.33}MnO_3$) [27], by Chahara *et al* ($La_{0.72}Ca_{0.25}MnO_3$) [28], and by Jin *et al* ($La_{1-x}Ca_xMnO_3$) [9]. These groups measured the MR associated with the transition from paramagnetic (PM) insulator to FM metal, and extended earlier work by Searle and Wang on $La_{1-x}Pb_xMnO_3$ [29]. The thin-film work was discussed in the framework of possible applicability of manganese perovskites to magnetic recording and Jin *et al* coined the term 'colossal magnetoresistance' [30] to draw a distinction between these oxides and the magnetoresistance found in 'giant magnetoresistance' (GMR) materials [1]. The latter are typically multilayer structures of alternating FM metal (e.g. Fe, Co) and normal metal (e.g. Cu) with layer thickness of order of the oscillation period of the RKKY interaction ($\approx$ Fermi wavevector). GMR occurs due to reversal of FM domains defined by the layer thickness. Because of the small field scales typically involved for these Heisenberg-like systems, the magnetoresistance is usually saturated at fields of order a few tenths of a tesla. Spin-valve and tunnelling techniques can reduce the field scale needed for a significant reduction in resistance to less than 0.01 T [31, 32], a region which allows application in magnetic reading devices. The field scale needed to achieve comparable resistance decreases in CMR compounds is much larger. Typical fields where the resitivity saturates are above 5 T. (Throughout, we will use the convention $MR_H = (R(0) - R(H))/R(H))$. Several ideas have been advanced to enhance the low-field MR in manganite perovskites and related CMR materials and these will be discussed in section 3.2.

2.3. Sr doping

Most of the recent work has focused on Ca- and Sr-substituted compounds and the CMR trends in encountered as a function of divalent ion concentration, x, are observed for both dopant types. However, there are some differences in the phase diagrams for the two cases, owing mainly to the size difference between Ca and Sr ions. For Sr substitution, Tokura and collaborators have established the phase behaviour as a function of x in melt-grown crystals of $La_{1-x}Sr_xMnO_3$ [33–36]. Ceramic samples have also been studied by Mahendiran *et al* [37] The phase boundaries are typically defined by inflection points in $M(T)$ data, the positions of which are shown as arrows in figure 2. As shown in figure 5(a), there are three distinct ground states: the spin-canted insulator, the FM insulator, and the FM metal. At high temperatures there appear to be two distinct phases, paramagnetic insulator (PI) and paramagnetic metal (PM). The vertical lines demarcating these phases are determined by crossover in $\rho(T)$ between semiconducting (insulating) and metallic behaviour, as shown in figure 5(a). Accompanying the insulator–metal transition at low temperature is an orthorhombic ($x \leqslant 0.175$) to rhombohedral ($x > 0.175$) transition. An important aspect of Sr substitution is the inability to obtain single-phase material for $x > 0.6$. Within the range of phase stability, however, there is a remarkably large variation in transport from good metal for $x > 0.3$ to insulator for $x \leqslant 0.15$. It should be noted that the crossover from metallic to insulating behaviour at $T = 0$ occurs in a very narrow concentration region. At the low end of the substitution series a remarkable field-induced structural transition is observed. As shown in figure 6, for $x = 0.17$, the orthorhombic–rhombohedral transition can be modified by about 50 K with application of a 7 T field [35].

Substitution on the La site modifies the phase behaviour through size effects (see section 2.8) as illustrated for $(Nd_{1-y}Sm_y)_{0.5}Sr_{0.5}MnO_3$ [38, 39]. This compound exhibits an instability towards either the FM ground state ($y = 0.875$, $T_C = 110$ K) or a high-ρ, low-M ($y = 0$, $T_{ins} = 160$) state, most likely either charge ordered or antiferromagnetic (or both). Similar behaviour is also found in $Pr_{0.5}Sr_{0.5}MnO_3$ [10] and $Pr_{0.7}(Sr, Ca)_{0.3}MnO_{3-\delta}$ [40, 41].

2.4. Ca doping

The phase diagram and low-temperature behaviour of $La_{1-x}Ca_xMnO_3$ was explored in detail [42–44] and is shown in figure 5(b). It is similar to that for Sr doping, especially in the region for $x < 0.5$. For $0.2 < x < 0.5$, the transition is defined by anomalies in $\rho(T)$ (figure 3), which move to higher temperature upon application of an applied magnetic field. Here one sees the origin of the CMR effect: the paramagnetic phase $\rho(T)$ is semiconducting and therefore, since T_C increases with H, the system undergoes an insulator–metal transition as H increases for fixed T. The high-field CMR is not sensitive to particle size in ceramic samples [45]. For $x > 0.5$, a well defined critical line with maximum around $T \approx 270$ K is seen in the T_C–x plane (figure 5(b)). This phase boundary defines the CO transition which is directly seen by TEM (figure 7). The low-temperature state in this doping regime was shown by Wollan and Koehler to be AF [11], and Ramirez *et al* [12] found evidence from bulk measurements, specific heat, $C(T)$, susceptibility $\chi(T)$, and sound velocity $v(T)$ for a an additional transition around $T \approx 170$ K which they ascribed to the AF transition. Later single-crystal work by Bao *et al* [46] on $Bi_{0.18}Ca_{0.82}MnO_3$ confirmed this assignment by showing the appearance of AF neutron diffraction peaks, clearly separated from the charge order features. Charge order is also seen in $La_{1-x}Ca_xMnO_3$ for $x \approx 0.51$ [42, 47]. Cheong *et al* studied the phase behaviour in $La_{1-x}Ca_xMnO_3$ by assigning maxima in dM/dT to

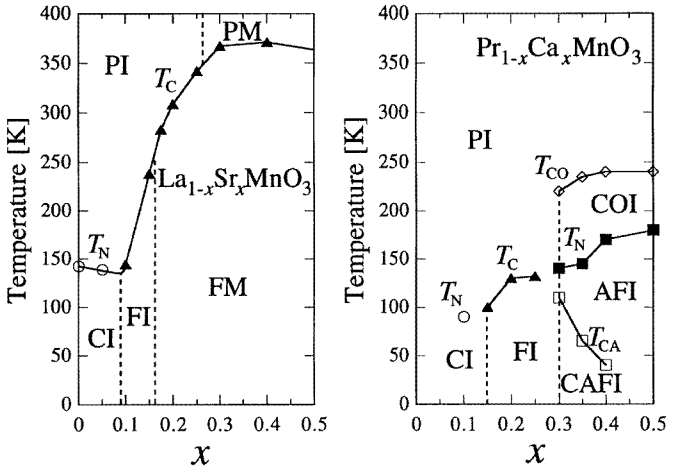

(a)

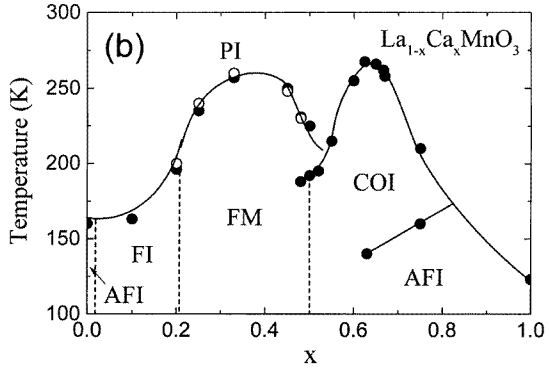

(b)

Figure 5. (a) Magnetic and electronic phase diagrams of $La_{1-x}Sr_xMnO_3$ and $Pr_{1-x}Ca_xMnO_3$. The various states are: paramagnetic insulating (PI), paramagnetic metal (PM), canted insulating (CI), ferromagnetic insulating (FI), ferromagnetic metal (FM), canted antiferromagnetic insulating (CAFI), and charge-ordered insulating (COI). T_C, T_N, and T_{CO}, are Curie, Néel, and charge-ordering temperatures, respectively. (b) Phases diagram for $La_{1-x}Ca_xMnO_3$. Labelling of phases is the same as in (a). (Reproduced from [49] (a) and [42] (b).)

either FM or CO transitions for samples with fine x resolution [44]. The authors find a maximum in the FM T_C of 272 K at $x = 3/8$. They also find a T_{CO} maximum of 265 K for $x = 5/8$. These data led the authors to suggest that both FM and CO are enhanced at commensurate values of the $2 \times 2 \times 2$ cubic Mn lattice. The behaviour for $x \approx 0.5$ is especially interesting. As depicted in figure 5(b), as the material is cooled from room temperature a FM state first develops, then followed by a CO/AF state which exhibits metamagnetic-like behaviour [48].

The phase diagram for $Pr_{1-x}Ca_xMnO_3$ was mapped out by Tomioka *et al* [49] for $x < 0.5$ (figure 5(a)). Because the Pr^{3+} ion is slightly smaller than La^{3+}, the phase behaviour also differs (see section 2.8). In single crystals, a succession of transitions from high-temperature charge ordering, to lower-temperature AF insulating and then canted AF states, were inferred from $\rho(T)$ data. Much attention has been paid to the compound

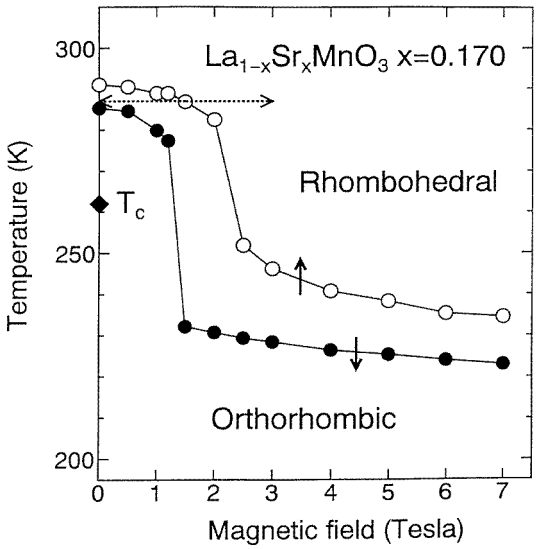

Figure 6. Structural phase diagram of $La_{1-x}Sr_xMnO_3$ ($x = 0.17$). The structural phase transition temperatures from the rhombohedral ($R\bar{3}c$) to orthorhombic ($Pbnm$) phase in the cooling run are shown by closed circles and open circles are obtained on warming. (Reproduced from [35].)

$Pr_{0.7}Ca_{0.3}MnO_3$ [50–52] which exhibits a first-order phase transition, in an applied magnetic field, at about 100 K between a low-temperature metallic and canted FM state and a higher-temperature insulating, AF and CO state. The most unusual aspect of this material is that on first cooling from room temperature to 4.2 K, metallic behaviour is not obtained until a field is applied. Application of a field of 5 T from a zero-field-cooled state leads to a change in resistance of nearly ten orders of magnitude.

2.5. Ba doping

Less work has been done on Ba-substituted phases. Thin films of $La_{0.67}Ba_{0.33}MnO_3$ were studied by von Helmolt *et al* [27]. Von Helmolt *et al* also studied [53] the series $La_{(2-x)/3}Ba_{(1+x)/3}Mn_{1-x}Cu_xO_3$ for which the end members of the series are the ferromagnetic $La_{2/3}Ba_{1/3}MnO_3$ and the superconducting $La_{1/3}Ba_{2/3}CuO_{7-\delta}$. In the Mn-rich region, the perovskite phase is found for $x < 0.4$. At $x = 0.3$, a semiconducting state appears with a spin-glass transition at $T \approx 50$ K. Ju *et al* studied $La_{0.67}Ba_{0.33}MnO_z$ as a function of oxygen content z [54]. It was found that on lowering z from 2.99 to 2.85, ρ increased by almost six orders of magnitude, uniformly over the temperature range 0–350 K (figure 8). Over the same composition range, the FM moment decreased by almost an order of magnitude. Note that for the purpose of determining the average Mn valence, reducing the O^{2-} concentration is equivalent to reducing the D cation concentration. For 30% D substitution of this series, the average Mn valence is driven back down to 3+ at $z = 2.835$. Hence, the difference between the ρ–M behaviour of $La_{0.67}Ba_{0.33}MnO_{2.85}$ (figure 8) and $LaMnO_3$, which exhibits pure semiconducting behaviour, might well be ascribed to oxygen disorder.

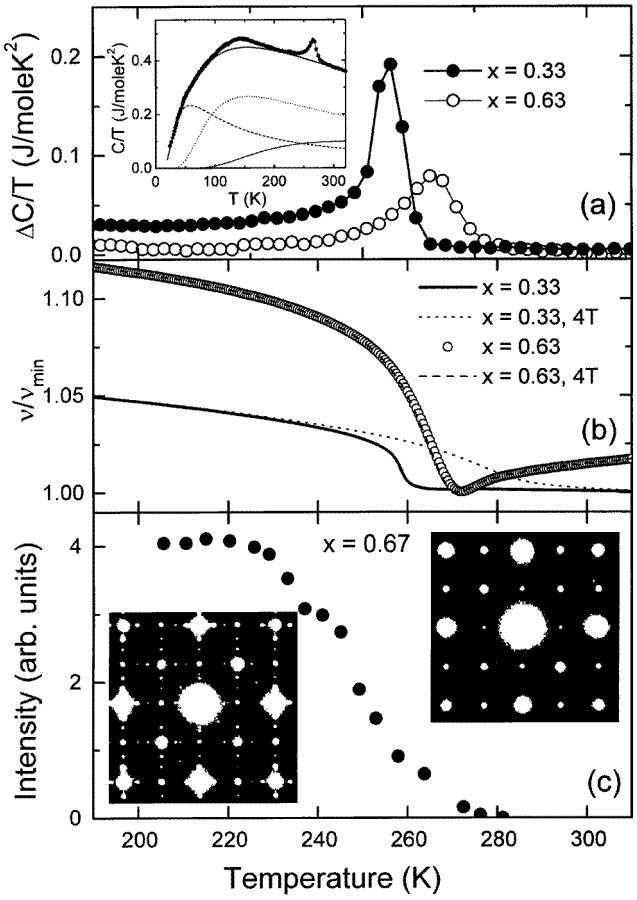

Figure 7. (a, inset) Specific heat divided by temperature, C/T, for $x = 0.63$. The lines are three optical mode phonon contributions and their sum, approximating the lattice contribution. (a) C/T for $x = 0.33$ and 0.63 with lattice contribution subtracted from each. (b) Sound velocity, v, for $x = 0.33$ and 0.63. The dashed lines are v in a field of 4 T. (c, insets) Electron diffraction patterns for $x = 0.67$ material. Charge ordering is seen as superlattice spots at 200 K (left) in addition to the main spots seen at 300 K (right). The main Bragg spots labelled a and b can be indexed as (200) and (020), respectively. (c) Intensity of a representative Bragg spot at $\delta \approx 0.33$ versus temperature. (Reproduced from [12].)

2.6. Layered compounds

The perovskite structure is one in a Ruddlesden–Popper series $(T_{1-x}D_x)_{n+1}Mn_nO_{3n+1}$ of layered compounds. Here, n indexes the number of connected layers of vertex-sharing MnO_6 octahedra. The endpoints in this series have $n = 1$ and ∞, which correspond to the single-layer K_2NiF_4 structure and the cubic perovskite structure, respectively. The $n = 1$ series of compounds $La_{1-x}Sr_{1+x}MnO_4$ has been well studied [55, 56]. These compounds exhibit insulating behaviour for all x, and in the region $x \approx 0.5$, a CO state appears below about $T = 250$ K [55–57]. At lower temperature ($T \approx 20$ K), a spin-glass state appears for $0.2 < x < 0.6$. Spin-glass behaviour is common among manganites with low T_C and presumably reflects the competition between the DE FM interaction and AF superexchange of the parent compound $LaMnO_3$. The $x < 0.1$ compounds are AF below $T \approx 100$ K.

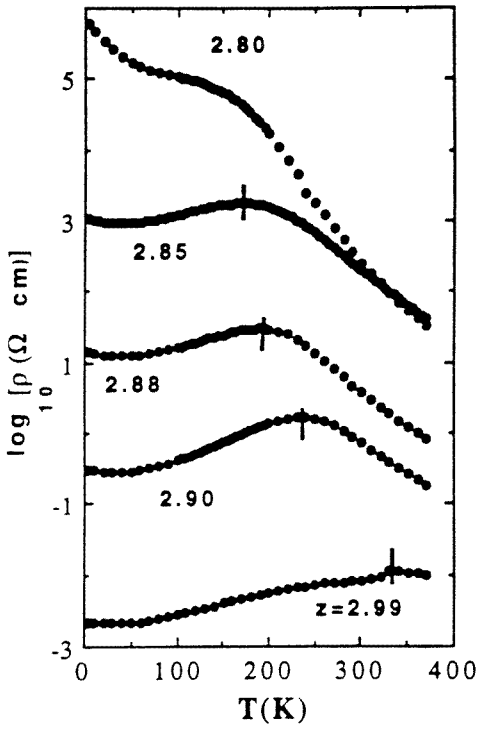

Figure 8. Temperature dependence of resistivity for $La_{0.67}Ba_{0.33}MnO_z$ ($2.80 \leqslant z \leqslant 2.99$). The vertical lines indicate resistivity peak positions. (Reproduced from [54].)

For $n = 2$, one has the so-called double-layer system. In these compounds large MR has also been observed for $La_{2-2x}Sr_{1+2x}Mn_2O_7$ [58] and $La_{2-2x}Ca_{1+2x}Mn_2O_7$ [59] (with this notation, x serves the same role as in the perovskites, denoting the nominal hole concentration). For Ca($x = 0.25$) a FM T_C of 215 K was identified but the MR peak occurs at a much lower temperature ~100 K. The discrepancy between these two temperatures was ascribed by the authors to the quasi-2D nature of the Mn–O layers. For Sr substitution, there are two transitions for $x = 0.4$, one at $T \approx 300$ K which can be attributed to 2D short-range order and a FM transition at $T = 126$ K, below which both c-axis and ab-plane resistivity change from semiconducting ($d\rho/dT < 0$) to metallic ($d\rho/dT > 0$). The MR for this compound is much larger than for the 3D ($n = \infty$) system which illustrates the general trend of increasing MR with decreasing T_C. At a slightly lower concentration, $x = 0.3$, the $n = 2$ system exhibits striking anisotropy in its transport properties; $d\rho_{ab}/dT > 0$ between the FM T_C and the 2D SRO T_C while $d\rho_c/dT < 0$ in the same temperature region (figure 9) [60]. That is, not only does the magnitude of $\rho(T)$ differ between the two principal crystallographic direction, but the form of the temperature dependence also differs. This decoupling of in-plane and out-of-plane transport behaviour is reminiscent of the highly anisotropic superconductors Sr_2RuO_4 and high-T_C cuprates. At low temperatures, large low-field MR is interpreted as interlayer tunnelling (section 3.2). The effect of different lanthanide-ion substitution has also been studied for the double-layer system for $LnSr_2Mn_2O_7$ [61, 62] which for Ln = Tb exhibits a low-temperature magnetization much reduced from that of Ln = La; for Ln = Nd, the magnetization is

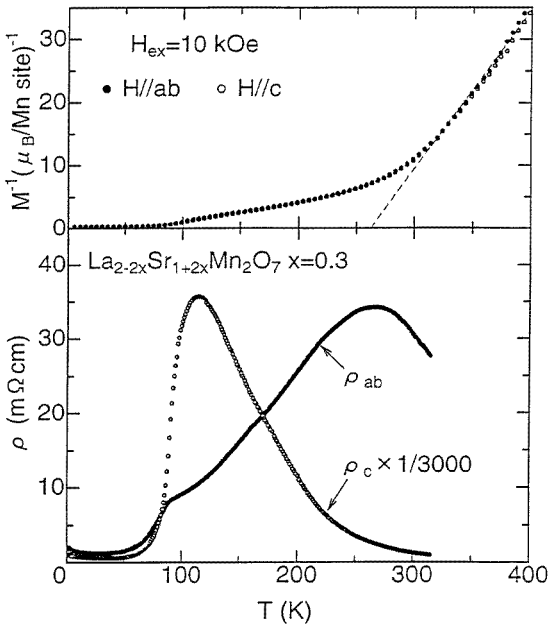

Figure 9. Top: temperature dependence of the inverse magnetization at $H = 1$ T. Bottom: in-plane (ρ_{ab}) and interplane (ρ_c) resistivity at zero field for the bilayer material $La_{2-2x}Sr_{1+2x}Mn_2O_7$ ($x = 0.3$) single crystal. (Reproduced from [60].)

also much smaller than for Ln = La, and hysteresis reminiscent of spin-glass ordering is seen near 150 K [63, 64]. A structural study for $0.5 \leqslant x \leqslant 0.75$ with Ln = La, Pr, Nd Sm, Eu, Gd, Tb, Dy, Ho, Y, and Er showed the existence of cation ordering between the two available cation sites with the smaller lanthanides preferring the site in between the double-layer block [65].

2.7. Bi-based compounds

The compound series $Bi_{1-x}Ca_xMnO_3$ has been studied by several groups [46, 66, 67]. Bismuth is stable in a trivalent state so one might expect behaviour similar to La-based systems. Interestingly, however, no evidence for metallicity ($d\rho/dT > 0$) has been found in polycrystalline samples for $0.3 < x < 0.9$ [66, 67] for $H = 0$. The absence of metallic behaviour can possibly be ascribed to the high polarizability of the Bi^{3+} ion. Chiba *et al* [67] report a FM state for $x > 0.8$ and a decrease in ρ ($T < 100$ K) by up to a factor of two in fields of 7 T for $x = 0.875$. For the latter composition, the ordered moment is only ∼50% of the theoretical Hund's-rule moment. Bao *et al* reported neutron diffraction on single crystals with $x = 0.82$ showing both CO and AF transitions [46]. Bismuth doping has also been studied in $(Sm, Sr)MnO_3$ [68].

2.8. Thin films

The influence of substrate strain is the main factor distinguishing manganite thin films from bulk ceramic samples. A commonly used substrate is $LaAlO_3$ which, though lattice matched to $(La, Ca)MnO_3$ at room temperature, strains the overlying film on reduction of T. Jin

et al have studied the effect of various substrates as well as film thickness on MR [69]. They find that the strain effect, expressed through the MR ratio (presumably also related to the reduction of T_C from that of bulk material of the same composition) is most pronounced for epitaxial films. They speculate that stress is most effectively propagated through the film thickness in the absence of grain boundaries. For $LaAlO_3$ substrate, MR is maximized for film thickness ≈1000 Å.

The composition dependence of MR has been studied by several groups, starting with von Helmolt *et al* [27], Chahara *et al* [28], and Jin *et al* [9]. Xiong *et al* found $MR_8 \approx 10^4$ at 60 K in $Nd_{0.7}Sr_{0.3}MnO_{3-\delta}$ films and showed how the MR was influenced by preparation conditions [70] ($MR_H \equiv (R(0) - R(H))/R(H)$). Xiong *et al* also showed that T_C of $La_{0.67}Ba_{0.33}MnO_3$ and $Nd_{0.67}Sr_{0.33}MnO_3$ films was reduced by a factor of two from the bulk values when deposition temperatures were raised to near 800 °C [71]. The T_C could then be raised by heat treating in an O_2 atmosphere or 1 h at 900 °C.

Epitaxial films of $La_{1-x}Ca_xMnO_3$ were grown on $SrTiO_3$ and $LaTiO_3$ substrates using ozone-assisted molecular beam epitaxy in a block-by-block deposition method [72]. A high degree of structural homogeneity was inferred for a $La_{0.58}Ca_{0.33}MnO_3$ film from extremely narrow rocking curve widths, showing the film to be fully strained. The magnetic transition at $T_C \approx 220$ K for this sample is broad, presumably due to the off-stoichiometry, which was determined after growth using inductively coupled plasma mass spectroscopy and Rutherford backscattering spectroscopy. Using a similar growth method, the same group grew $La_{0.67}Ca_{0.33}MnO_{3-\delta}$ films with a root-mean-square surface roughness of only 2 Å [73]. The magnetic transition at $T_C \approx 170$ K is substantially sharper than the off-stoichiometry film.

Films of $La_{0.67}Ca_{0.33}MnO_3$ and $La_{0.67}Sr_{0.33}MnO_3$ with $\rho(T)$ and $M(T)$ very similar to bulk behaviour were grown by Snyder *et al* using solid source chemical vapour deposition on $LaAlO_3$ substrates [74]. In a separate study, this group showed that repeated annealing between 660 K and 1200 K in flowing argon gas progressively lowered the resistivity of a $La_{0.67}Ca_{0.33}MnO_3$ film, uniformly over the range 80 to 1200 K [75]. This suggests to the authors that films as grown by the MOCVD technique do not suffer so much from oxygen off-stoichiometry as from oxygen disorder.

2.9. Bandwidth versus bandfilling—structure systematics and pressure studies

The compounds described above are of course all related to each other on a microscopic level. From the point of view of single-band conduction, the two parameters defining this relationship are band filling and band width (W). In the phase diagrams depicted in figure 5, x variation represents variation of Mn d^3 site density and, in turn, hole concentration and bandfilling are varied. Alternatively, the average size of the A cation, $\langle r_A \rangle$, in the ABO_3 formula can be varied. This will alter the lattice constant and thus the one-electron bandwidth. Hwang *et al* have systematically studied the evolution of T_C in the compounds $La_{0.7-y}Pr_yCa_{0.3}MnO_3$ and $La_{0.7-y}Y_yCa_{0.3}MnO_3$ while keeping the Ca concentration fixed [76]. They found that a decreasing $\langle r_A \rangle$ corresponds to a decreasing T_C as shown in figure 10. Similar conclusions are reached by Fontcuberta *et al* [77] and Maignan *et al* [78]. This behaviour is also seen for the AF transition in the insulating phases of $RNiO_3$ where R is a rare-earth ion [79].

The experiments which vary internal pressure by varying lanthanide radius, $\langle r_A \rangle$, are complemented by studies where external hydrostatic pressure is varied. Moritomo *et al* performed resistivity measurements up to 18 kbar on $La_{1-x}Sr_xMnO_3$ ($0.15 \leqslant x \leqslant 0.5$) [80]. They find that dt_C/dP ($t_C \equiv T_C(P) - T_C(0)$) strongly varies as a function of concentration. They note that the itinerant ferromagnet $SrRuO_3$ displays behaviour of similar magnitude

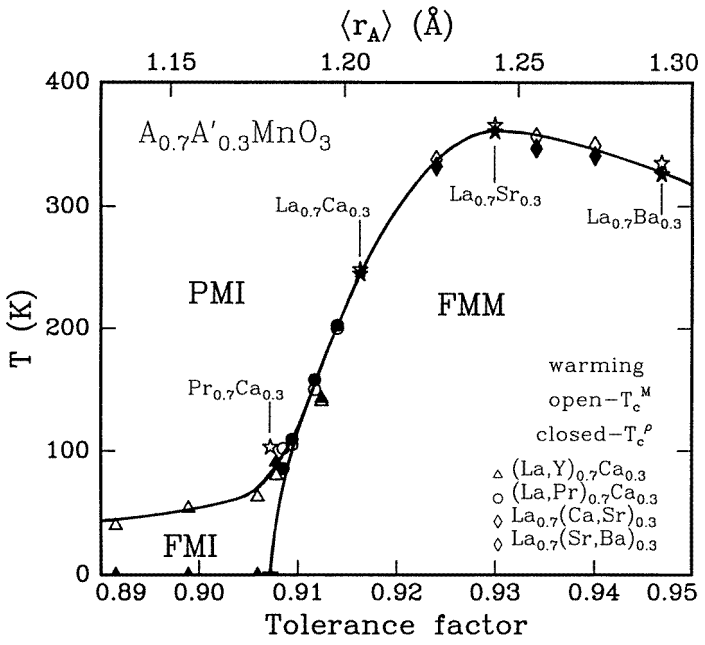

Figure 10. Phase diagram of temperature versus tolerance factor for $A_{0.7}A'_{0.3}MnO_3$, where A is a trivalent ion and A′ a divalent ion. Open symbols denote T_C determined by magnetization measurements and closed symbols denote T_C determined by resistivity measurements. All data were taken while warming. (Reproduced from [76].)

but opposite sign [81], suggesting that DE is not the dominant interaction determining T_C. Khazeni studied $Nd_{0.5}Sr_{0.36}Pb_{0.14}MnO_{3-\delta}$ single crystals ($T_C \simeq 170$ K) [82]. They find that both T_C determined from resistivity and the MR peak shift up by about 2 K kbar^{-1} for 10.5 kbar. Similar dT_C/dP values are found by Neumeier *et al* for polycrystalline samples of $La_{1-x}Ca_xMnO_3$ ($x = 0.21$, 0.33, 0.40) [83] and Zhou *et al* [84]. The latter study also reports thermopower as function of pressure. The increase of dT_C/dP as x decreases is presumably related to an increasing sensitivity of T_C to internal pressure, as is evident in figure 10. Hwang *et al* performed a similar study on $Pr_{0.7}Ca_{0.3}MnO_3$ and $La_{0.7}Ca_{0.3}MnO_3$ and made direct contact to their internal pressure studies [85]. They conclude that both applying external pressure and increasing the rare-earth average radius, $\langle r_A \rangle$ tilt the MnO_6 octahedra, so the Mn–O–Mn bond approaches 180° thus increasing the matrix element for transport. The interplay of structure and electronic transport is also evident in a study of the compressibility of the Mn–O bond angle for the bilayer system $La_{1.2}Sr_{1.8}Mn_2O_7$ [86]. Here it is found that in the FM state, the Mn–O–Mn distance expands under applied pressure whereas it contracts in the paramagnetic state, behaviour which is interpreted in terms of exchange striction and the competition between double exchange and superexchange.

In both internal and external pressure studies, decreasing $\langle r_A \rangle$ decreases the Mn–O–Mn bond angle away from 180°, thus reducing the electron hopping matrix element and consequently the bandwidth. Thus, the $\langle r_A \rangle$–T_C relationship is consistent with a transition which is driven by the kinetic energy gain of the carriers on entering the metallic state. The theory of Millis *et al* addresses the trends on varying x and $\langle r_A \rangle$ and argues that the e–ph couping constant λ is the crucial parameter controlling T_C: increasing λ decreases T_C [13]. Although the intent of the experimental work is to vary only either the bandfilling, or W, through x

and $\langle r_A \rangle$ respectively, in fact the experiments vary both at the same time. For Ca concentration variation, clearly $\langle r_A \rangle$ is not fixed. Similarly, for the $\langle r_A \rangle$–T_C experiments, although x is held constant it is quite likely that the *effective* filling changes as the e–ph coupling varies. To view the interconnected nature of the experimental parameters in terms of a discussion of microscopic variables, it is useful to plot T_C values for the various phases on a plot of x and $\langle r_A \rangle$, as shown in figure 11. Here we see that FM ground states are obtained in a bounded region of x–$\langle r_A \rangle$ space bounded above by the large size of La^{3+}, and below by a series of transitions into CO, AF, and spin-glass states which are strongly coupled to lattice distortions as expected from an increasingly influential λ. This plot suggests that MR and T_C are connected by a 'universal' relationship. The fact that large MR values occur for small T_C values is not surprising for two reasons: first, since the transition to a metallic state is from a semiconducting-like state and hence the lower is T_C, the larger is ρ just above T_C and in turn $\Delta\rho$ on entering the metallic state; second, the higher T_C, the greater the contribution from scattering due to phonons, magnons, and other electrons, which will set a lower bound on ρ in the metallic state and hence an upper bound on MR. The universal MR–T_C relationship among many different manganite–perovskite CMR systems is shown by Khazeni *et al* in figure 12 [82]. This relationship seems to place a natural limit on MR in the perovskites, and thus motivates searches for large MR among other compound families.

2.10. Pyrochlores

The basic CMR phenomena have also been observed in the compound $Tl_2Mn_2O_7$ with pyrochlore structure. In this cubic structure MnO_6 octahedra are corner sharing, forming a sparse network intersecting with a network of Tl–O chains. These materials can only be synthesized under high pressure and therefore are much less studied. Shimakawa *et al* first noted the CMR behaviour, a FM transition at $T \approx 170$ K with a concurrent reduction in $\rho(T)$, and a large $MR_5 \approx 3$ near T_C [19]. Cheong *et al* studied the effect of In substitution and found little change in MR for $x < 0.25$ in $Tl_{2-x}In_xMn_2O_7$ [87]. Above this concentration, the material becomes multiphase but also exhibits a much larger CMR. Subramanian *et al* demonstrated, using neutron and single-crystal x-ray diffraction, that CMR is intrinsic to the stoichiometric compound [88]. This work discriminated the pyrochlore CMR mechanism from that of the perovskites. The latter are AF when not intentionally doped and only exhibit metallicity and a FM moment for large admixtures of Mn^{4+} in the $LaMnO_3$ parent compound. Another important difference between the two materials is that $Tl_2Mn_2O_7$ is metallic above T_C whereas the perovskites are insulating. Ramirez and Subramanian showed that with Sc substitution, the MR_6 grows by factor of 60, while T_C decreases only by 15% [89]. This large increase in MR_6 is accompanied by a transition from metallic behaviour for the pure compound $Tl_2Mn_2O_7$ to semiconducting behaviour for $Tl_{1.8}Sc_{0.2}Mn_2O_7$. These studies, taken together, suggest that the FM ordering is not driven by kinetic energy gain associated with the insulator–metal transition but rather from a type of 'FM' superexchange. Subramanian *et al* suggested that CMR in this compound is best described by spin-fluctuation scattering between localized Mn^{4+} moments and the conduction band which originates from the 6s electrons on the Tl–O sublattice. This idea is further supported by band structure calculations [90–92].

Ramirez *et al* have demonstrated moderately large high-field magnetoresistance in the Cr chalcogenide spinels $Fe_{1-x}Cu_xCr_2S_4$ [20]. These compounds are similar to the Tl–Mn pyrochlores in that the A-site ion can contribute to states near the Fermi level. This property, along with the flexibility of substitution on the A site of many different ionic species, leads to good potential for future materials work.

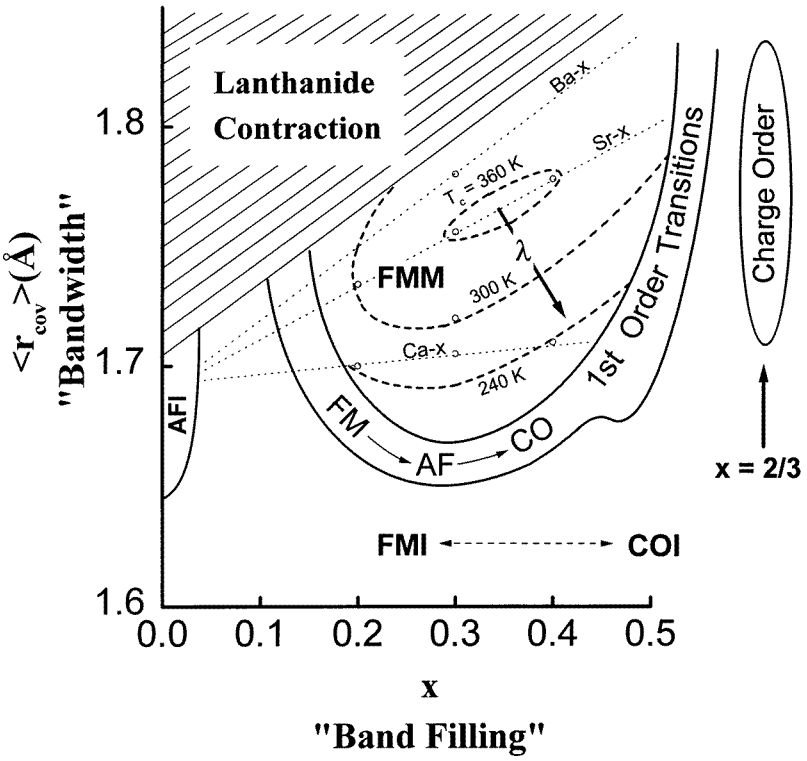

Figure 11. Phase diagram in the plane defined by average A-site covalent radius, $\langle r_{cov} \rangle$, and divalent ion concentration, x, showing the various antiferromagnetic insulating (AFI), ferromagnetic metal (FMM), ferromagnetic insulator (FMI), and charge-ordered insulating (COI) phases. Inside the region labelled FMM, values of T_C are shown. The dashed lines show the effect of Sr, Ca, and Ba substitution. The bold arrow indicates that the electron–phonon coupling, λ, as discussed in [13], increases as T_C decreases. Charge order is most stable near $x = 0.5$ and $x = 0.6$–0.67.

3. Transport

3.1. High-temperature transport in perovskites—evidence for polarons

A discussion of the phenomenology of electronic transport in the manganite perovskites can be conveniently separated into three regimes, high-temperature, low-temperature, and critical region. Critical behaviour is best described by thermodynamic measurements which couple directly to the magnetic correlation length. There does not yet exist a full complement of data to address the criticial behaviour (but see section 4.1). We therefore restrict the discussion to behaviour at low and high temperatures.

3.1.1. High-temperature resistivity, thermopower. At high temperature, $T > T_C$, in the concentration region where CMR is strongest, $0.2 < x < 0.4$, transport is characterized by an activated resistivity, $\rho(T) \propto \exp(\Delta_\rho/T)$ [3] where $\Delta_\rho \approx$ 1000–2000 K (other reported values are 1100 ± 60 K for $Nd_{0.5}Pb_{0.5}MnO_3$ [26], 1300 K on $La_{0.67}Ca_{0.33}MnO_3$ thin film [93], 2500–1000 K for $La_{1-x}Ca_xMnO_3$ $0.1 < x < 0.6$ [94], depending on x). The thermopower, $S(T)$, also behaves as expected for a semiconductor, $S(T) \propto \Delta_S/T$, where

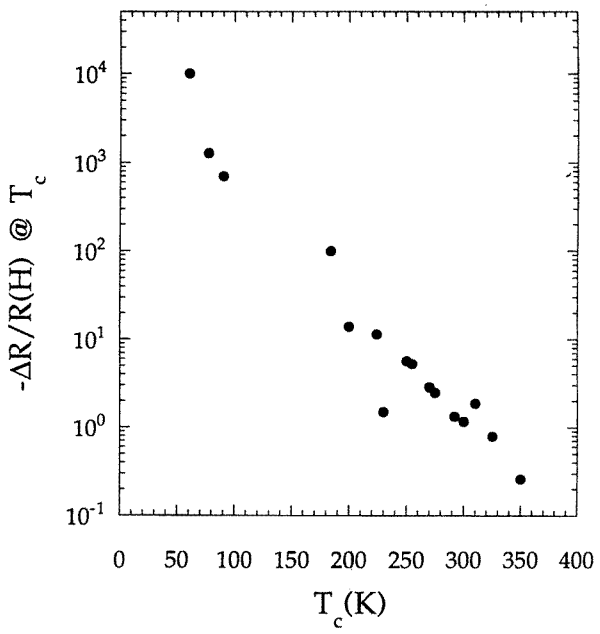

Figure 12. Maximum MR_{5-12} versus T_C, compiled for a variety of different manganese oxide perovskite compounds (reproduced from [82]).

$\Delta_S \approx 120$ K [93], 500–20 K [94–100] (figure 13). In the simplest of models, namely that of an intrinsic semiconductor with a single carrier type, $\Delta_\rho = \Delta_S$. The experimental work indicates an order-of-magnitude discrepancy between Δ_ρ and Δ_S, which strongly suggests an additional excitation. It has been suggested, based on the size of the lattice distortion associated with the Jahn–Teller effect for d^4 ions with octahedral coordination, that charge conduction is via small polarons. In the extreme case of noninteracting polarons, there is no entropy transport accompanying charge transport since the polaron energy term in the chemical potential cancels the polaron energy term in the high-temperature expansion of the Kubo formula [101]. In the presence of polaron–polaron interactions, however, this cancellation does not occur and an extra contribution, of the order of the interaction strength, appears. Thus in this scenario, Δ_ρ measures the polaron binding energy while Δ_S measures the polaron–polaron interaction energy. Additional terms will include a spin entropy term, $S_s = (k_B/e)\ln(4/5) \approx 20\ \mu\text{V K}^{-1}$, and a configurational (Heikes) entropy term, $S_c = (k_B/\text{e})\ln\{(1-c_h)/c_h\}$, where c_h is the fractional hole concentration. It is observed that at high temperatures, $S(T)$ extrapolates to a value consistent with S_s, independent of x, presenting a puzzle which is perhaps related to the difference between Δ_S and Δ_ρ. The thermopower of $La_{0.67}Ca_{0.33}MnO_3$ films in an applied field undergoes the behaviour expected from the known T_C shift and in the critical region displays decreases greater than a factor of 10 for H up to 8 T.

An alternative, chemistry-based, interpretation of thermopower which seeks to explain the anomalous x-independence at high temperatures is offered by Hundley and Neumeier [100]. The implication that the configurational term, S_c, is nearly x independent is contrary to the expectation that substitution of one Ca ion leads to one mobile hole. They point out that usually $Mn^{3+}(3d^4)$ is less stable than its neighbours, $Mn^{2+}(3d^5)$ and $Mn^{4+}(3d^3)$, and this can lead to disproportionation of Mn^{3+}–Mn^{3+} pairs into Mn^{2+}–Mn^{4+} pairs, a

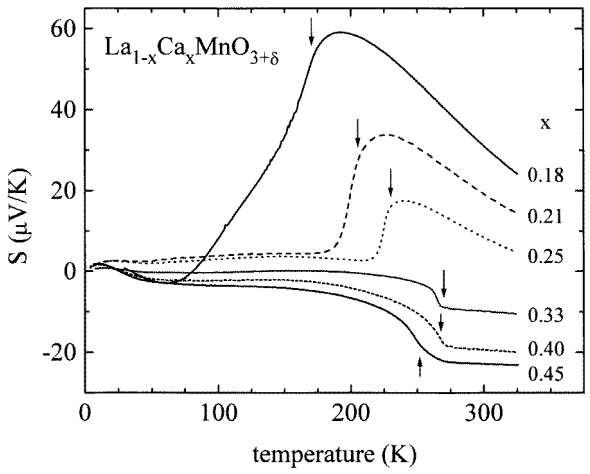

Figure 13. The Seebeck coefficient for $La_{1-x}Ca_xMnO_{3+\delta}$ with varying Ca^{2+} concentration. The arrows indicate the magnetic ordering temperature. (Reproduced from [100].)

phenomenon not uncommon in transition metal oxides. If one then postulates that only one of the several different Mn valence species is conducive to polaron hopping, then as x is varied, not only is the number of carriers varied, but also the number of possible sites for transport. The configurational contribution, S_c, would therefore depend on the disproportionation probability of Mn^{3+} and after correcting the for this using existing thermal-gravinometric (TGA) data, good agreement is found with the Heikes formula. This provides an important alternative view of conduction in the manganites which should be addressed further.

The Hall effect in thin films of $(La_{1-y}Gd_y)_{0.67}Ca_{0.33}MnO_3$ have been measured by Jaime *et al* [102]. (Gd substitution is used here to lower $T_C \approx 130$ K.) In the paramagnetic region the carrier sign is negative. This is argued to result from hopping processes involving odd-numbered Aharonov–Bohm loops, which means, for the perovskites, that next-nearest-neighbour hopping processes dominate charge transport. Measurements of the Hall effect both above and below T_C were carried out on $La_{1-x}Ca_xMnO_3$ films with $T_C \approx 260$ K by Matl *et al* [103]. They find in the FM phase a carrier density $n \approx 1$ hole/Mn site, or about three times the Ca concentration. Near T_C the carrier sign changes to electron-like in agreement with the results of Jaime *et al*. The authors report the surprising result that the mobility, $B^{-1}\tan\theta$, where B is the magnetic induction and θ the Hall angle, is field independent near T_C and for fields up to a few tesla. This implies that CMR is due to a field-induced increase in the carrier density. This result seems in conflict with the double-exchange view where changes in $\rho(T)$ are due to changes in scattering rate, via the magnetization.

3.2. Low-temperature transport—low-field magnetoresistance

The low-temperature transport can be divided into two distinct phenomena, the behaviour of the intrinsic, metallic or semiconducting, state which characterizes high-field MR, and that of the intergrain process which characterizes the low-field behaviour.

3.2.1. Low-temperature resistivity—intergrain transport, noise. Ju *et al* noticed large low-field magnetoresistance ($MR_{0.3} = 25\%$) in ceramic samples of $La_{0.67}Ba_{0.33}MnO_z$ ($z = 2.99$,

2.90) and ascribed this to transport across magnetic domain boundaries [54]. Schiffer *et al* observed the same effect in ceramic $La_{0.75}Ca_{0.25}MnO_3$, ($MR_{0.2} = 45\%$ at 0.2 T) [42]. In this experiment, however, the size of the residual resistivity, $\rho_0 = 10^{-3}$ Ω cm implied a mean free path of ∼10 Å, much smaller than a typical domain size, leading the authors to suggest an additional source of scattering in the grain boundaries. Hwang *et al* demonstrated that this effect was in fact due to scattering by grain boundaries by comparing the low-field MR of polycrystalline $La_{0.67}Sr_{0.33}MnO_3$ and single crystals of the same composition, for which the low-field effect is absent [104] (figure 14). They showed that the magnitude of the initial drop in $\rho(H)$ varies with temperature as $[a + b/(T + c)]$ which is characteristic of spin-polarized tunnelling in granular ferromagnets [31, 105]. Gupta *et al* correlated the low-field MR in films of $La_{0.67}D_{0.33}MnO_{3-\delta}$ (D = Ca, Sr or vacancies) with grain size as measured using transmission electron microscopy (TEM) [106]. They observed no low-field MR for epitaxial films and a $MR_{0.5} = 25\%$ at 25 K for films with 3 μm grain size. Trilayer devices with junction structure, $La_{0.67}Sr_{0.33}MnO_3/SrTiO_3/La_{0.67}Sr_{0.33}MnO_3$ show $R_{0.01} \approx 83\%$ at 4.2 K [107]. Tunnelling has been directly observed in these devices as a nonlinear I–V characteristic [108].

Mathur *et al* have fabricated a device that probes the effect of transport across a single grain boundary [109]. They use a bicrystal $SrTiO_3$ substrate on which is grown a 200 nm epitaxial (002) $La_{0.7}Ca_{0.3}MnO_3$ film. A meander line is then patterned from the film across the grain boundary formed at the bicrystal junction. The section of material spanning the grain boundary is one arm of an *in situ* Wheatstone bridge to further isolate the behaviour of the defect. A peak in the effective resistance of the defect is seen just below T_C and associated with this is an effective $MR_{0.18}$ which decreases to zero at T_C in a nearly linear fashion. This magnitude of the low-field MR at temperatures close to 300 K is larger than that reported by Hwang *et al* [104] in polycrystalline material and demonstrates the feasibility of room-temperature devices made from CMR material. Finally Hwang *et al* have achieved large MR at low field using a 'heterostructure' made of $La_{0.67}Ca_{0.33}MnO_3$ sandwiched between two pole pieces of a soft ferromagnet ($(Mn, Zn)Fe_2O_4$) [110]. Here the applied field is enhanced by the internal field of the pole pieces so the demagnetization field is expected to play an important role in application of this concept to devices.

Central to any discussion of usefulness of CMR materials is whether the MR signal is large compared to the intrinsic noise. Issues of concern are both the high $\rho(T_C)$ values and the $1/f$ noise related to magnetic domain fluctuations. Alers *et al* have addressed these issues with noise measurements in $La_{0.6}Y_{0.07}Ca_{0.33}MnO_3$ thin films [111]. These films had a $MR_6 > 10^3$ at $T_C = 180$ K. The noise was typically $1/f$ in character and, when averaged over the frequency band 1 = 25 Hz, had a broad maximum as a function of temperature, peaking below T_C. Due to the $1/f$ character, low-frequency applications near T_C are constrained—the equivalent magnetic field noise for a volume of 10^{-12} cm^3, is roughly 10^3 Oe Hz^{-1}. However, at high frequencies, e.g. 10 MHz, the signal to noise ratio for a 1 Oe signal is roughly 20 dB. Thus, while domain-related noise might inhibit incorporation of CMR material for low-frequency applications, such as magnetic storage, these problems are reduced singificantly for high-frequency applications such as reading.

3.2.2. Low-temperature resistivity—intrinsic. The inherent cation disorder in the solid solution manganites can lead to electronic scattering which results in large values of $\rho_0 \equiv \rho(T = 0)$. Nevertheless, several groups have addressed the intrinsic scattering mechanisms. Of relevance here is the prediction of $\rho(T) \propto T^{4.5}$ for electron–magnon scattering in a double-exchange system [112]. Schiffer *et al* found in $La_{1-x}Ca_xMnO_3$ for

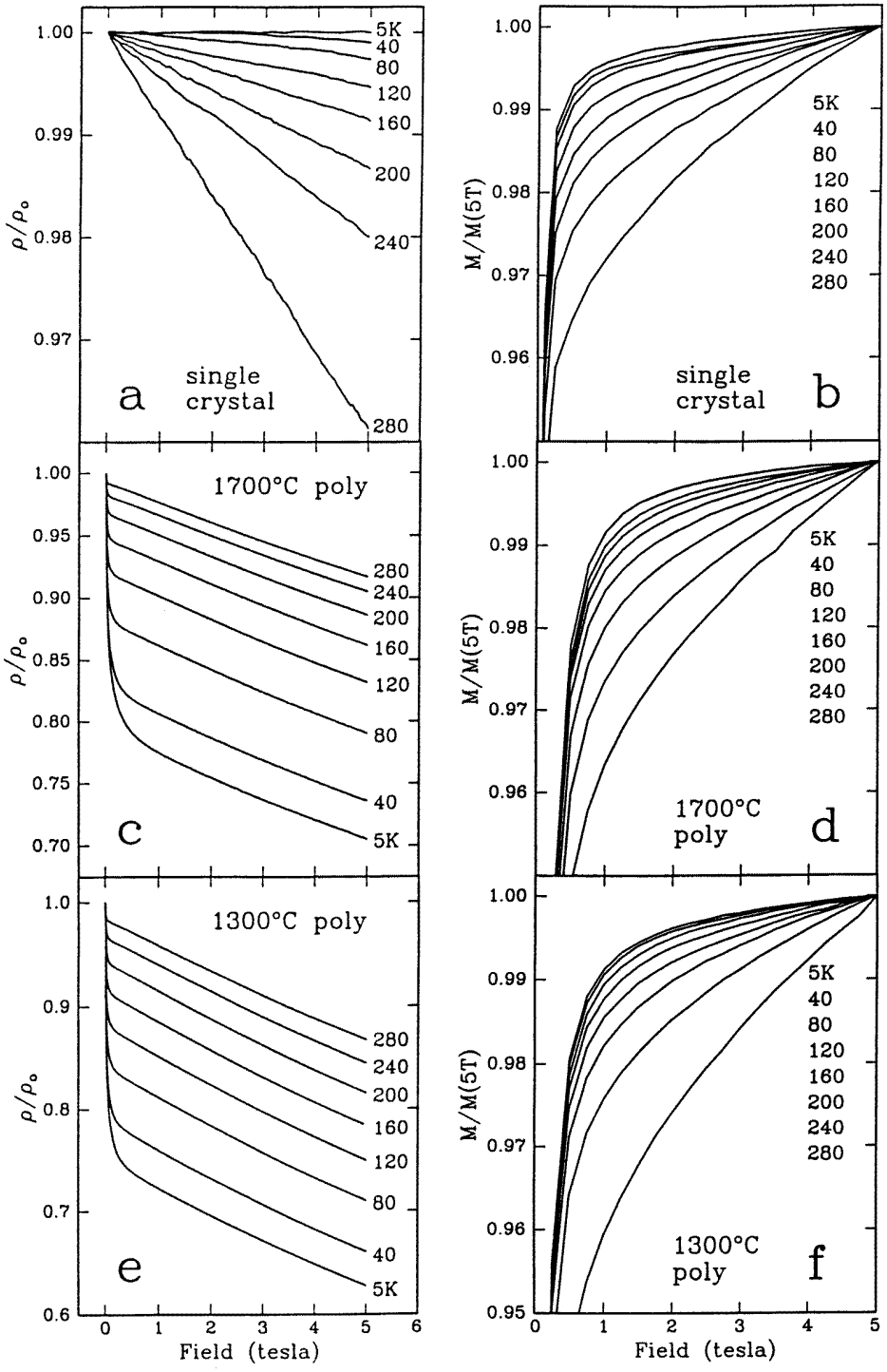

Figure 14. Panels a, c, and e: the magnetic field dependence of the normalized resistance at various temperatures from 5 to 280 K. Panels b, d, and f: the magnetic field dependence of the magnetization (normalized to the 5 T value) at various temperatures from 5 to 280 K. (Reproduced from [104].)

$x = 0.20$, 0.33, 0.45, that the resistivity for $T < 0.5T_C$ is well fitted by the expression $\rho(T) = \rho_0 + \rho_1 T^p$, where $p = 2.5$, whereas $p = 4.5$ provides a poor fit [42]. However, the data can be fitted by the above expression using $p = 4.5$ and an additional T^2 term representing electron–electron scattering. A similar conclusion was reached by Snyder *et al* based on measurements of $\rho(T)$ in high-quality films of $La_{0.67}D_{0.33}MnO_3$ (D = Ca, Sr) where ρ_0 values as small as 100 Ω cm were achieved [113]. Urushibara *et al* plot $\rho(T) - \rho_0$ versus T^2 for $T < 200$ K for $La_{1-x}Sr_xMnO_3$ ($x = 0.3$, 0.4) crystals possessing $\rho_0 < 100$ μΩ cm [33]. They find upward curvature on such a plot, consistent with Schiffer *et al*. These characteristic temperature dependences should not be automatically assumed to indicate only electron–electron and electron–magnon scattering since at the temperatures over which the fits are made (10–150 K), electron–phonon scattering can be significant since $\theta_D \approx 400$–500 K. Finally, small ρ_0 values with intrinsic $\rho(T)$ behaviour are also seen in single crystals of $Pr_{0.5}Sr_{0.5}MnO_3$ which on cooling in zero field exhibit semiconducting-like $d\rho/dT < 0$ [10]. On application of fields of order 7 T, $\rho(T)$ is converted to that of a metal, $d\rho/dT > 0$ and ρ_0 can be as low as 150 μΩ cm. The studies which concentrate on the intrinsic $\rho(T)$ behaviour at low temperatures support the view that there are several contributions and that further work is needed, especially at temperatures below 1 K in grain-boundary-free material, to determine the relative strengths of different scattering mechanisms.

3.3. Optical conductivity

The optical conductivity was studied by Okimoto *et al* [114] on single-crystal $La_{1-x}Sr_xMnO_3$ ($x = 0.175$). As shown in figure 15, the main effect of the transition to the metallic state is to shift spectral weight from an energy much higher than accessed in the experiment to a Drude-like contribution below 1 eV. In addition to this is a broad peak centred at about 1.4 eV. Similar results are found in thin-film $Nd_{0.7}Sr_{0.3}MnO_3$ with a significantly lower T_C (≈180 K) by Kaplan *et al* [115]. These authors measured transmittance and reflectance to obtain the optical conductivity from 15 K to 300 K and up to 8.9 T. A shift of spectral weight from above 1 eV to below 1 eV occurs as metallicity is induced either with decreasing T or increasing H. A broad peak similar to that seen by Okimoto *et al* is also seen and it is argued that the main contribution to this peak comes from a charge-transfer transition from a Jahn–Teller-split Mn^{3+} e_g level to an unoccupied Mn^{4+} e_g level on an adjacent site. It is likely that the energy of this process is related to the polaron binding energy. Arima and Tokura performed an study of the optical reflectivity of RMO_3 (R = La, Y; M = Sc, Ti, V, Cr, Mn, Fe, Co, Ni, Cu) [116]. They observe a charge gap for most compounds. In particular, for $LaMnO_3$, no feature is seen in the 1 eV range as for the doped materials, supporting the polaron interpretation of Kaplan *et al*.

4. Magnetic and lattice probes

4.1. Neutrons, μSR probing magnetic order

Wollan and Koehler performed neutron scattering measurements on polycrystalline specimens of $La_{1-x}Ca_xMnO_{3+\delta}$ [11]. They observed that as x is varied away from 0.3, the FM moment decreases and AF Bragg reflections appear. Five different AF ordered states are observed, depending on x. In the region $x \sim 0.5$, a mixture of two AF patterns, along with FM scattering, is observed. The multiple electronic states for $x = 0.5$ have been studied by Radaelli *et al* [117]. They find that in the temperature region between the FM and

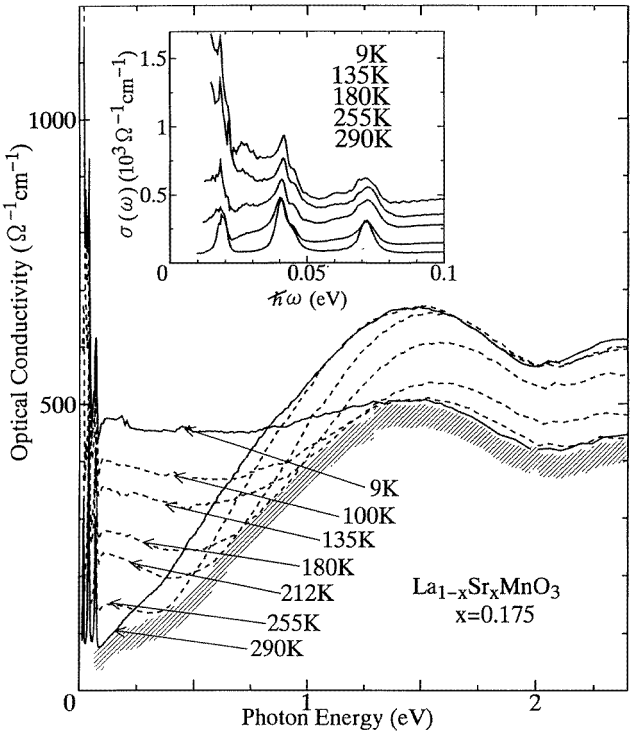

Figure 15. Optical conductivity spectra of $La_{1-x}Sr_xMnO_3$ ($x = 0.175$ and $T_C = 238$) at various temperatures. The hatched curve represents the temperature-independent part of the spectra deduced from the envelope of the respective curves. The inset shows a magnification of the far-infrared part. (Reproduced from reference [114].)

COI phase boundaries depicted in figure 5(b), there are short-range antiferromagnetic Bragg peaks, suggestive of a model of Goodenough [21] which describes ordering of J–T-distorted sites (orbital ordering). At the same time, there is an unusual broadening of structural Bragg reflections which suggests the crystal passes through a number of intemediate orbitally ordered phases before selecting the low-temperature orthorhombic structure. Jirak *et al* performed neutron scattering measurements on $Pr_{1-x}Ca_xMnO_3$ for a variety of x values [22]. They noted that below room temperature there exist four distinct structural regimes as a function of x: $x < 0.3$ orthorhombic, $0.3 < x < 0.7$ tetragonal (compressed), $0.75 < x < 0.9$ tetragonal (elongated), $x > 0.9$ pseudo-cubic. Magnetically ordered states similar to those found by Wollan and Koehler were observed. Charge-ordered states, as predicted by Goodenough [21], were also observed.

Several recent studies have elaborated on these early works; Yoshizawa *et al* studied the metal–insulator transition in $Pr_{0.7}Ca_{0.3}MnO_3$ [51]; Moussa *et al* measured the spin wave dispersion of $LaMnO_3$ ($T_N = 139.5$ K) but here an admixture of FM and AF interactions defines a magnetic structure in which spins order in FM planes with AF interplane correlations [118].

Inelastic neutron scattering was used by Perring *et al* to measure the spin wave dispersion throughout the Brillouin zone of single-crystal $La_{0.7}Pb_{0.3}MnO_3$ ($T_C = 355$) [119]. These authors found that the spin wave energies are described by the simplest possible FM dispersion with a magnon bandwidth of $\sim$100 meV. The authors point out the

surprising simplicity of this description, given that both the parent compound $LaMnO_3$, and neighbouring chemical phases, are AF. One would expect there to be softening near zone boundaries even for small admixtures of AF interaction.

Using inelastic scattering, Lynn *et al* measured the dispersion relation for polycrystalline $La_{0.67}Ca_{0.33}MnO_3$ [120]. Writing the long-wavelength spin wave dispersion relation as $E = \Delta + D(T)q^2$, they find a spin stiffness that does not vanish at T_C ($D(0) = 170$ meV Å^2, $D(250) = 80$ Å^2). In addition, in intensity–energy scans at $q = 0.07$ Å, they observe a central peak with a width broader than the spin wave peaks. This implies the existence of quasistatic excitations (polarons?) which elastically scatter neutrons.

Inelastic scattering has also been performed on the bilayer material $La_{1.2}Sr_{1.8}Mn_2O_7$ by Perring *et al* [121]. In addition to a peak in FM scattering seen at $T_C = 126$ K, there is also a broad peak feature extending over the temperature range 120–200 K where zone boundary, i.e. AF, scattering ($\boldsymbol{Q} = (0.5, 0, 0)$) is observed. The maximum correlation length extracted from the AF Bragg scattering peaks is $\xi = 9.3 \pm 1.3$ Å at $T = 150$ K, and $\xi = 6.7 \pm 2.2$ Å even at 300 K. Since electronic hopping is suppressed on a local scale when neighbouring spins are antiparallel, these data illustrate that, at least for this 2D material, localization due to a random placement of the AF clusters (Anderson localization) must be included in a microscopic theory of transport.

4.1.1. μSR. Muon spin relaxation (μSR) probes the internal field at the muon stopping site. Heffner *et al* have performed zero-field μSR experiments on polycrystalline $La_{0.67}Ca_{0.33}MnO_3$ [122]. They find that the sublattice magnetization varies as $(1 - T/T_C)^{\beta}$ where $\beta = 0.345 \pm 0.015$ for $T < T_C$. This is in accord with a continuous 3D phase of the XY universality class ($\beta = 0.38$, 0.33, 0.31 for 3D Heisenberg, XY, and Ising systems respectively). In addition, for $T \leqslant T_C$, the muon relaxation varies as $\exp(-(\Lambda t)^{1/2})$ instead of the usual form $\exp(-\Lambda t)$. This behaviour has been seen in spin-glass alloys and suggests to the authors that the spin dynamics below T_C are non-ergodic. Interestingly, although spin-glass effects have not been observed by the traditional means (e.g. time-dependent dc-magnetization effects), spin-glass-like hysteresis has been seen in magnetization measurements of $La_{0.7-y}Pr_yCa_{0.3}MnO_3$ for $x > 0.5$, concentrations which reduce T_C to below 150 K [76].

4.2. Neutron probes of lattice excitations

In a discussion of the two generic ground states seen in the manganite perovskites, ferromagnetism and charge order, lattice excitations play a key role. One of the first indications of this role is in the measurement by Dai *et al* of the neutron cross section for coherent elastic scattering [16]. This is proportional to $\exp(-2W)$ where W is the Debye–Waller factor, $2W(\boldsymbol{Q}) = \langle(\boldsymbol{Q} \cdot \boldsymbol{u})^2\rangle$ where the rms nuclear displacement is $\langle \boldsymbol{u}^2 \rangle$. $\langle \boldsymbol{u}^2 \rangle$ for every atom in $La_{0.65}Ca_{0.35}MnO_3$ varies very strongly with temperature as shown in figure 16. To see how anomalous this variation is, the authors related it to anharmonic lattice distortions via the Grüneisen coefficient, $\gamma = \mathrm{d}\ln\omega/\mathrm{d}V$, where ω is an average acoustic phonon energy, and V the unit-cell volume. Using $W(T_2)/W(T_1) = [V(T_2)/V(T_1)]^{2\gamma_{eff}}$, the authors find γ_{eff} varies from ~85 (260–40 K) to ~25 (600 and 260 K). This is to be compared to typical γ values in the range 2–3 in most solids and clearly shows that anharmonic lattice modes are present in the manganite perovskites. Similar results are also reported by Radaelli *et al* [123].

These Debye–Waller measurements are complemented by studies of the neutron scattering pair distribution function (PDF) by Billinge *et al* [124]. These measurements

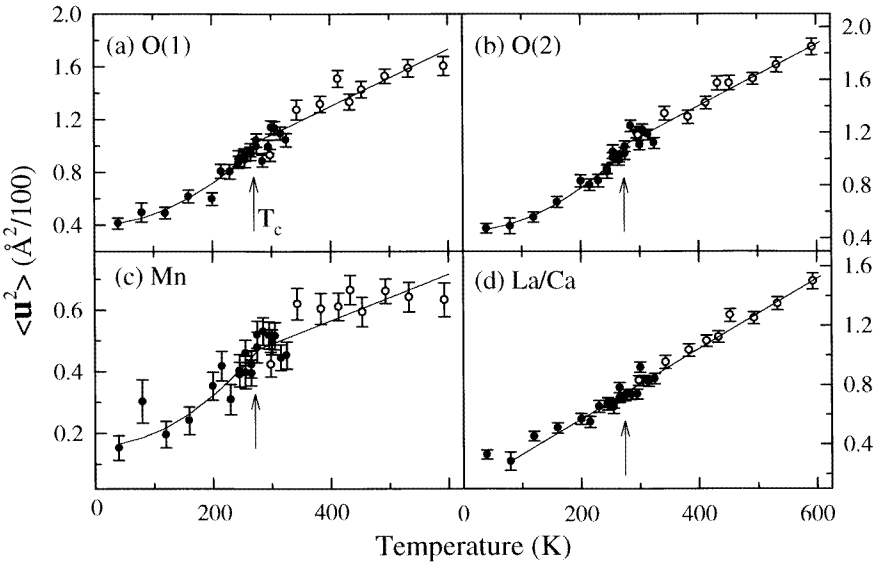

Figure 16. Isotropic Debye–Waller factors for different atoms in the perovskite $La_{0.65}Ca_{0.35}MnO_3$ against T, as obtained from Reitveld refinements. O(1)–Mn and O(2)–Mn bonds are along the b axis and in the a–c plane, respectively (*Pnma* space group). Solid lines are to guide the eye. (Reproduced from [16].)

probe the local structure and show for $La_{1-x}Ca_xMnO_3$ ($x = 0.20$, 0.25) a transition from a high-temperature state with disordered Mn–O and O–O bond lengths to a low-temperature state with a uniform bond length distribution. The bond disorder is ascribed to electron hopping, involving real-space displacement of large Jahn–Teller-distorted (d^4) Mn–O octahedra by undistorted (d^3) octahedra. In the FM state, on the other hand, the carriers are delocalized and any distortion will be uniformly averaged over Mn–O sites.

4.3. Specific heat, thermal conductivity

The specific heat, $C(T)$, of $La_{0.8}Ca_{0.2}MnO_3$ has been measured by Tanaka and Mitsuhashi [125] between 100 and 300 K. A sharp anomaly is observed at 206 K and a small fraction (10%) of the expected entropy, $\sim$11 J mol^{-1} K^{-1}, is found to reside under an ordering peak. Approximately twice as much entropy was found to reside under the ordering peak in $La_{0.67}Ca_{0.33}MnO_3$ by Ramirez *et al* [12]. This shortfall of entropy has several possible explanations, the most obvious one being that the background subtraction is not accurate enough to fully account for the short-range order entropy developed above T_C. The second explanation is that the transition does not correspond to a reduction of only local-moment degrees of freedom. In addition, there is expected to be an entropy gain in the ordered state, due to the delocalization of electrons. Ramirez *et al* estimate that this gain can be as much as 25% of the local moment contribution. These authors also measured $C(T)$ for a range of concentrations from $x = 0.1$ to 0.9 and observed peaks corresponding to charge order (with roughly the same entropy as seen for the FM transition) at $x = 0.63$–0.65, and $C(T)$ which is hysteretic upon warming and cooling for $x = 0.5$.

The low-temperature $C(T)$ of the manganite perovskites has been measured by several groups [126–128] Woodfield *et al* studied $La_{1-x}Sr_xMnO_3$ for $x = 0$, 0.1, 0.2, and 0.3 from

$T = 0.5$ to 10 K [128]. They show that $C(T)$ has contributions from four distinct sources: spin waves, conduction electrons, phonons, and nuclear moments. The latter is especially important due to the large internal fields in these materials and properly accounting for this term is necessary to extract accurate fit parameters for the other three terms. Of particular interest is the electronic γ coefficient which is found to be approximately 3.2 mJ mol^{-1} K^{-2} for $x = 0.2$, 0.3 and zero for $x = 0$, 0.1, clearly demonstrating the metal–insulator transition already implied by resistance measurements.

4.3.1. Thermal conductivity. The thermal conductivity, $\kappa(T)$, of polycrystalline $La_{1-x}Ca_xMnO_3$ ($x = 0.1$ and 0.3) and single-crystal $La_{0.2}Nd_{0.4}Pb_{0.4}MnO_3$ and $La_{0.6}Pb_{0.4}MnO_3$ have been measured by Visser *et al* [129]. They find the surprising result that, in the paramagnetic phase and for $T \approx \theta_D$, $\kappa(T)$ is a monotonically increasing function of temperature, up to 380 K. This is contrary to what is expected for crystalline insulators, where $\kappa = Cvl$, and the high-temperature behaviour is dominated by $l \propto 1/T$ (v is the phonon group velocity, and C approaches the Dulong–Petit constant, C_{DP}). Instead, the behaviour is closer to amorphous systems where l is a constant, fixed to a structural correlation length, and the weak increase of $\kappa(T)$ with T reflects $C(T)$. Although the samples studied included single crystals, the analogy to amorphous behaviour is perhaps not superficial, given the PDF and Debye–Waller measurements described above. The authors argue that the unusual $\kappa(T)$ arises from phonon scattering dominated by the strongly anharmonic lattice modes and related to the Debye–Waller factor via the relation $\kappa \propto aMC_{DP}\theta_D^3/\gamma^2 T$, where a is the lattice constant and M the mass per atom. Thus, in the paramagnetic state the manganites have the unusual property that they are *disordered* at short lengths but *ordered* at long lengths. In addition, there is an observed 30% increase in $\kappa(T_C = 260$ K) in a field of 6 T for $La_{0.2}Nd_{0.4}Pb_0.4MnO_3$. This increase cannot be related to the decrease in ρ via a Wiedemann–Franz relation, a result which underscores the importance of electron–phonon coupling for electron transport.

4.4. Isotope effect

One of the most intriguing experiments performed on the manganite perovskites is the isotope effect of Zhao *et al* [15]. Here, the FM T_C is measured before and after exchanging ^{18}O for ^{16}O (95% of full exchange) by dc magnetization. Zhao *et al* find a reduction of T_C by 20 K for $La_{0.8}Ca_{0.2}MnO_3$ from a starting value of about 210 K for ^{16}O. This was contrasted to the absence of a shift observed for the itinerant ferromagnetic $SrRuO_3$ where 80% exchange was achieved. This large T_C shift on varying the oxygen mass is not yet explained by theory, and is most likely related to the magnetism via modification of a J–T polaron mass. This shows dramatically the effect of phonons on a transition which up to recently was widely viewed as purely electronic in origin.

5. Summary and outlook

Colossal magnetoresistance in the manganite perovskites is only one facet of a complex many-body phenomenon. The combined metal–insulator and ferro–paramagnetic transition and its description in terms of a double-exchange interaction provide the starting point for a microscopic description of the various ground states. To this has been added electron–lattice coupling, starting from a single-ion Jahn–Teller effect. The electron–phonon coupling, in providing the basis for a polaron description of the high-temperature transport,

is a key element of CMR. But there are many other ramifications of strong electron–phonon coupling in manganite perovskites among which are charge order, magnetic-field-dependent structural transitions, large Debye–Waller factors, anomalous thermal conductivity temperature dependence, and the isotope effect. Although a good understanding of CMR has been achieved, these other phenomena are much less well understood. Of particular interest is a detailed understanding of the metal–insulator critical behaviour at low temperatures.

An important motivation for studying CMR is the potential for applications. Here, the sought-after feature is large, e.g. 50%, MR at low, e.g. 10 Oe, field and room temperature. The initial flurry of activity was brought about by reports of large MR at high field and low temperature. Recently, through a sequence of ingenious experiments on manganite perovskites, it is now possible to achieve 5% MR at 1800 Oe at 247 K, and there is every reason to expect this figure of merit to increase to challenge GMR in the near future. Large MR is, however, only one property of a useful device and future work will need to address, for example, issues involving power consumption, noise, and compatibility with established fabrication methods.

Finally, there have been efforts to find compounds with features similar to the perovskites, and these searches have led us to the pyrochlore and spinel-based materials. Whether these materials will compete with the perovskites near room temperature remains to be seen. What they will certainly provide is new insight into magneto-transport near metal–insulator boundaries.

Acknowledgments

I would like to acknowledge my collaborators in CMR. In this regard I thank especially P Schiffer. I also thank P Littlewood, A Millis, P Majumdar, and B Shraiman for many helpful discussions. I am grateful to G Ernst, P Majumdar, and P Schiffer for careful readings of the manuscript.

References

[1] Parkin S P P 1995 *Annu. Rev. Mater. Sci.* **25** 357
[2] Goodenough J B 1976 *Magnetism and the Chemical Bond* (Huntington: Krieger)
[3] Jonker G H and Van Santen J H 1950 *Physica* **16** 337
[4] Van Santen J H and Jonker G H 1950 *Physica* **16** 599
[5] Zener C 1951 *Phys. Rev.* **81** 440
[6] Anderson P W and Hasegawa H 1955 *Phys. Rev.* **100** 675
[7] De Gennes P-G 1960 *Phys. Rev.* **118** 141
[8] Millis A J, Littlewood P B and Shraiman B I 1955 *Phys. Rev. Lett.* **74** 5144
[9] Jin S, Tiefel T H, McCormack M, Fastnacht R A, Ramesh R and Chen J H 1994 *Science* **264** 413
[10] Tomioka Y, Asamitsu A, Moritomo Y, Kuwahara H and Tokura Y 1955 *Phys. Rev. Lett.* **74** 5108
[11] Wollan E O and Koehler W C 1955 *Phys. Rev.* **100** 545
[12] Ramirez A P, Schiffer P, Cheong S-W, Bao W, Palstra T T M, Gammel P L, Bishop D J and Zegarski B 1996 *Phys. Rev. Lett.* **76** 3188
[13] Millis A J, Shraiman B I and Mueller R 1996 *Phys. Rev. Lett.* **77** 175
[14] Röder H, Zhang J and Bishop A R 1996 *Phys. Rev. Lett.* **76** 1356
[15] Zhao G, Conder K, Keller H and Müller K A 1996 *Nature* **381** 676
[16] Dai P, Zhang J, Mook H A, Liou S-H, Dowben P A and Plummer E W 1996 *Phys. Rev.* B **54** R3694
[17] Fletcher J R and Stephens K W H 1969 *J. Phys. C: Solid State Phys.* **2** 444
[18] Elemans J B A A, Van Laar B, Van Der Veen K R and Loopstra B O 1971 *J. Solid State Chem.* **3** 238
[19] Shimakawa Y, Kubo Y and Manako T 1996 *Nature* **379** 53
[20] Ramirez A P, Cava R J and Krajewski J 1997 *Nature* **387** 268

[21] Goodenough J B 1955 *Phys. Rev.* **100** 564
[22] Jirak Z, Krupicka S, Simsa Z, Dlouha M and Vratislav S 1985 *J. Magn. Magn. Mater.* **53** 153
[23] Varma C M 1996 *Phys. Rev.* B **54** 7328
[24] Satpathy S, Popovic Z S and Vukajlovic F R 1996 *Phys. Rev. Lett.* **76** 960
[25] Park J-H, Chen C T, Cheong S-W, Bao W, Meigs G, Chakarian V and Idzerda Y U 1996 *Phys. Rev. Lett.* **76** 4215
[26] Kusters R M, Singleton J, Keen D A, McGreevy R and Hayes W 1989 *Physica* B **155** 362
[27] von Helmolt R, Wecker J, Holzapfel B, Schultz L and Samwer K 1993 *Phys. Rev. Lett.* **71** 2331
[28] Chahara K, Ohno T, Kasai M and Kozono Y 1993 *Appl. Phys. Lett.* **63** 1990
[29] Searle C W and Wang S T 1969 *Can. J. Phys.* **47** 2703
Searle C W and Wang S T 1970 *Can. J. Phys.* **48** 2023
[30] Jin S, McCormack M, Tiefel T H and Ramesh R 1994 *J. Appl. Phys.* **76** 6929
[31] Helman J S and Abeles B 1976 *Phys. Rev. Lett.* **37** 1429
[32] Moodera J S, Kinder L R, Wong T M and Meservey R 1995 *Phys. Rev. Lett.* **74** 3273
[33] Urushibara A, Moritomo Y, Arima T, Asamitsu A, Kido G and Tokura Y 1995 *Phys. Rev.* B **51** 14 103
[34] Tokura Y, Urushibara A, Moritomo Y, Arima T, Asamitsu A, Kido G and Furukawa N 1994 *J. Phys. Soc. Japan* **63** 3931
[35] Asamitsu A, Moritomo Y, Tomioka Y, Arima T and Tokura Y 1995 *Nature* **373** 407
[36] Kuwahara H, Tomioka Y, Asamitsu A, Moritomo Y and Tokura Y 1995 *Science* **270** 961
[37] Mahendiran R, Raychaudhuri A K, Chainani A, Sarma D D and Roy S B 1995 *Appl. Phys. Lett.* **66** 233
[38] Tokura Y, Kuwahara H, Moritomo Y, Tomioka Y and Asamitsu A 1996 *Phys. Rev. Lett.* **76** 3184
[39] Caignaert V, Maignan A and Raveau B 1995 *Solid State Commun.* **95** 357
[40] Raveau B, Maignan A and Caignaert V 1995 *J. Solid State Chem.* **117** 424
[41] Maignan A, Simon Ch, Caignaert V and Raveau B 1996 *J. Magn. Magn. Mater.* **152** L5
[42] Schiffer P, Ramirez A P, Bao W and Cheong S-W 1995 *Phys. Rev. Lett.* **75** 3336
[43] Gong G Q, Canedy C, Xiao G, Sun J Z, Gupta A and Gallagher W J 1995 *Appl. Phys. Lett.* **67** 1783
Gong G Q, Gupta A, Xiao G, Lecoeur P and McGuire T R 1996 *Phys. Rev.* B **54** R3742
[44] Cheong S-W, Lopez C M and Hwang H Y 1997 *Preprint*
[45] Mahesh R, Mahendiran R, Raychaudhuri A K and Rao C N R 1996 *Appl. Phys. Lett.* **68** 2291
[46] Bao W, Axe J D, Chen C H and Cheong S-W 1997 *Phys. Rev. Lett.* **78** 543
[47] Chen C H and Cheong S-W 1996 *Phys. Rev. Lett.* **76** 4042
[48] Xiao G, McNiff E J Jr, Gong G Q, Gupta A, Canedy C L and Sun J Z 1996 *Phys. Rev.* B **54** 6073
[49] Tomioka Y, Asamitsu A, Kuwahara H, Moritomo Y and Tokura Y 1996 *Phys. Rev.* B **53** R1689
[50] Barratt J, Lees M R, Balakrishnan G and Paul D McK 1996 *Appl. Phys. Lett.* **68** 424
[51] Yoshizawa H, Kawano H, Tomioka Y and Tokura Y 1995 *Phys. Rev.* B **52** R13145
[52] Yoshizawa H, Kawano H, Tomioka Y and Tokura Y 1996 *J. Phys. Soc. Japan* **65** 1043
[53] von Helmolt R, Haupt L, Bärner K and Sondermann U 1992 *Solid State Commun.* **82** 641
[54] Ju H L, Gopalakrishnan J, Peng J L, Li Q, Xiong G C, Venkatesan T and Greene R L 1995 *Phys. Rev.* B **51** 6143
[55] Moritomo Y, Tomioka Y, Asamitsu A, Tokura Y and Matsui Y 1995 *Phys. Rev.* B **51** 3297
[56] Bao W, Chen C H, Carter S A and Cheong S-W 1996 *Solid State Commun.* **98** 55
[57] Sternlieb B J, Hill J P, Wildgruber U C, Luke G M, Nachumi B, Moritomo Y and Tokura Y 1996 *Phys. Rev. Lett.* **76** 2169
[58] Moritomo Y, Asamitsu A, Kuwahara H and Tokura Y 1996 *Nature* **380** 141
[59] Asano H, Hayakawa J and Matsui M 1996 *Appl. Phys. Lett.* **68** 3638
[60] Kimura T, Tomioka Y, Kuwahara H, Asamitsu A, Tamura M and Tokura Y 1996 *Science* **274** 1698
[61] Battle P D, Green M A, Laskey N S, Millburn J E, Rosseinsky M J, Sullivan S P and Vente J F 1996 *Chem. Commun.* **1996** 767
[62] Seshadri R, Martin C, Maignan A, Hervieu M, Raveau C and Rao C N R 1996 *J. Mater. Chem.* **6** 1585
[63] Battle P D *et al* 1996 *J. Phys.: Condens. Matter* **8** L427
[64] Battle P D, Green M A, Laskey N S, Milburn J E, Radaelli P G, Rosseinsky M J, Sullivan S P and Vente J F 1996 *Phys. Rev.* B **54** 15 967
[65] Battle P D, Green M A, Laskey N S, Millburn J E, Murphy L, Rosseinsky M J, Sullivan S P and Vente J F 1997 *Chem. Mater.* **9** 552
[66] Bokov V A, Grigoryan N A and Bryzhina M F 1967 *Phys. Status Solidi* **20** 745
[67] Chiba H, Kikuchi M, Muraoka Y and Syono Y 1996 *Solid State Commun.* **99** 499
[68] Damay F, Maignan A, Hervieu M, Nguyen N and Raveau B 1996 *C. R. Acad. Sci. Paris* **322** 573
[69] Jin S, Tiefel T H, McCormack M, O'Bryan H M, Chen L H, Ramesh R and Schurig D 1995 *Appl. Phys. Lett.* **67** 557

[70] Xiong G C, Li Q, Ju H L, Mao S N, Senapati L, Xi X X, Greene R L and Venkatesan T 1995 *Appl. Phys. Lett.* **66** 1427
[71] Xiong G C, Li Q, Ju H L, Greene R L and Venkatesan T 1995 *Appl. Phys. Lett.* **66** 1689
[72] Achutharaman V S, Kraus P A, Vas'ko V A, Nordman C A and Goldman A M 1995 *Appl. Phys. Lett.* **67** 1019
[73] Vas'ko V A, Nordman C A, Kraus P A, Achutharaman V S, Ruosi A R and Goldman A M 1996 *Appl. Phys. Lett.* **68** 2571
[74] Snyder G J, Hiskes R, DiCarolis S, Beasley M R and Geballe T H 1996 *Phys. Rev.* B **53** 14 434
[75] Worledge D C, Snyder G J, Beasley M R, Geballe T H, Hiskes R and DiCarolis S 1996 *J. Appl. Phys.* **80** 1
[76] Hwang H Y, Cheong S-W, Radaelli P G, Marezio M and Batlogg B 1995 *Phys. Rev. Lett.* **75** 914
[77] Fontcuberta J, Martinez B, Seffar A, Piñol S, García-Muñoz J L and Obradors X 1996 *Phys. Rev. Lett.* **76** 1122
[78] Maignan A, Simon Ch, Caignaert V and Raveau B 1996 *Z. Phys.* B **99** 305
[79] Torrance J B, Lacorre P, Nazzal A I, Ansaldo E J and Niedermayer Ch 1992 *Phys. Rev.* B **45** 8209
[80] Moritomo Y, Asamitsu A and Tokura Y 1995 *Phys. Rev.* B **51** 16 491
[81] Shikano M, Huang T, Inaguma Y, Itho M and Nakamura T 1994 *Solid State Commun.* **90** 115
[82] Khazeni K, Jia Y X, Lu L, Crespi V H, Cohen M L and Zettl A 1996 *Phys. Rev. Lett.* **76** 295
[83] Neumeier J J, Hundley M F, Thompson J D and Heffner R H 1995 *Phys. Rev.* B **52** R7006
[84] Zhou J-S, Archibald W and Goodenough J B 1996 *Nature* **381** 770
[85] Hwang H, Palstra T T M, Cheong S-W and Batlogg B 1995 *Phys. Rev.* B **52** 15 046
[86] Argyriou D N, Mitchell J F, Goodenough J B, Chmaissem O, Short S and Jorgensen J D 1997 *Phys. Rev. Lett.* **78** 1568
[87] Cheong S-W, Hwang H Y, Batlogg B and Rupp L W Jr 1996 *Solid State Commun.* **98** 163
[88] Subramanian M A, Toby B H, Ramirez A P, Marshall W J, Sleight A W and Kwei G H 1996 *Science* **273** 81
[89] Ramirez A P and Subramanian M A 1997 *Science* **277** 546
[90] Seo D-K, Whangbo M-H and Subramanian M A 1997 *Solid State Commun.* **101** 417
[91] Singh D J 1997 *Phys. Rev.* B **55** 313
[92] Matar S F, Subramanian M A and Etourneau J *J. Mater. Chem.* at press
[93] Jaime M, Salamon M B, Rubinstein M, Treece R E, Horwitz J S and Chrisey D B 1996 *Phys. Rev.* B **54** 11 914
[94] Palstra T T M, Ramirez A P, Cheong S-W, Zegarski B R, Schiffer P and Zaanen J 1996 unpublished
[95] Miller R C, Heikes R R and Mazelsky R 1961 *J. Appl. Phys.* **32** (Supplement 2202)
[96] Fontcuberta J, Seffar A, Granados X, Garcia-Munoz J L, Obradors X and Pinol S 1996 *Appl. Phys. Lett.* **68** 2288
[97] Asamitsu A, Moritomo Y and Tokura Y 1996 *Phys. Rev.* B **53** R2952
[98] Hashimoto T, Ishizawa N, Mizutani N and Kato M 1988 *J. Mater. Res.* **23** 1102
[99] Jaime M, Salamon M B, Pettit K, Rubinstein M, Treece R E, Horwitz J S and Chrisey D B 1996 *Appl. Phys. Lett.* **68** 1576
[100] Hundley M F and Neumeier J J 1997 *Phys. Rev.* B **55** 11 511
[101] Girvin S M 1978 *J. Solid State Chem.* **25** 65
[102] Jaime M, Hardner H T, Salamon M B, Rubinstein M, Dorsey P and Emin D 1997 *Phys. Rev. Lett.* **78** 951
[103] Matl P, Yan Y F, Ong N P, Li Y Q, Studebaker D, Baum T and Doubinina G 1996 *Preprint*
[104] Hwang H Y, Cheong S-W, Ong N P and Batlogg B 1996 *Phys. Rev. Lett.* **77** 2041
[105] Berkowitz A E, Mitchell J R, Carey M J, Young A P, Zhang S, Spada F E, Parker F T, Hutten A and Thomas G 1992 *Phys. Rev. Lett.* **68** 3745
[106] Gupta A, Gong G Q, Xiao G, Duncombe P R, Lecoeur P, Trouilloud P, Wang Y Y, Dravid V P and Sun J Z 1996 *Phys. Rev.* B **54** R15629
[107] Sun J Z, Gallagher W J, Duncombe P R, Krusin-Elbaum L, Altman R A, Gupta A, Lu Y, Gong G Q and Xiao G 1996 *Appl. Phys. Lett.* **69** 3266
[108] Lu Y, Li X W, Gong G Q, Xiao G, Gupta A, Lecoeur P, Sun J Z, Wang Y Y and Dravid V P 1996 *Phys. Rev.* B **54** R8357
[109] Mathur N D, Burnell G, Isaac S P, Jackson T J, Teo B-S, MacManus-Driscoll J L, Cohen L F, Evetts J E and Blamire M G 1997 *Nature* **387** 266
[110] Hwang H Y, Cheong S-W and Batlogg B 1996 *Appl. Phys. Lett.* **68** 3494
[111] Alers G B, Ramirez A P and Jin S 1996 *Appl. Phys. Lett.* **68** 3644
[112] Kubo K and Ohata N 1972 *J. Phys. Soc. Japan* **33** 21
[113] Snyder G J, Hiskes R, DiCarolis S, Beasley M R and Geballe T H 1996 *Phys. Rev.* B **53** 14 434
[114] Okimoto Y, Katsufuji T, Ishikawa T, Urushibara A, Arima T and Tokura Y 1995 *Phys. Rev. Lett.* **75** 109

[115] Kaplan S G, Quijada M, Drew H D, Tanner D B, Xiong G C, Ramesh R, Kwon C and Venkatesan T 1996 *Phys. Rev. Lett.* **77** 2081
[116] Arima T and Tokura Y 1995 *J. Phys. Soc. Japan* **64** 2488
[117] Radaelli P G, Cox D E, Marezio M, Schiffer P E and Ramirez A P 1995 *Phys. Rev. Lett.* **75** 4488
[118] Moussa F, Hennion M, Rodriguez-Carvajal J, Moudden H, Pinsard L and Revcholevschi A 1996 *Phys. Rev.* B **54** 15 149
[119] Perring T G, Aeppli G, Hayden S M, Carter S A, Remeika J P and Cheong S-W 1996 *Phys. Rev. Lett.* **77** 711
[120] Lynn J W, Erwin R W, Borchers J A, Huang Q, Santoro A, Peng J-L and Li Z Y 1996 *Phys. Rev. Lett.* **76** 4046
[121] Perring T G, Aeppli G, Moritomo Y and Tokura Y 1997 *Phys. Rev. Lett.* **78** 3197
[122] Heffner R H, Le L P, Hundley M F, Neumeier J J, Luke G M, Kojima K, Nachumi B, Uemura Y J, MacLaughlin D E and Cheong S-W 1996 *Phys. Rev. Lett.* **77** 1869
[123] Radaelli P G, Marezio M, Hwang H Y, Cheong S-W and Batlogg B 1996 *Phys. Rev.* B **54** 8992
[124] Billinge S J L, DiFrancesco R G, Kwei G H, Neumeier J J and Thompson J D 1996 *Phys. Rev. Lett.* **77** 715
[125] Tanaka J and Mitsuhashi T 1984 *J. Phys. Soc. Japan* **53** 24
[126] Coey J M D, Viret M, Ranno L and Ounadjela K 1995 *Phys. Rev. Lett.* **75** 3910
[127] Hamilton J J, Keatley E L, Ju H L, Raychaudhuri A K, Smolyaninova V N and Greene R L 1996 *Phys. Rev.* B **54** 14 926
[128] Woodfield B F, Wilson M L and Byers J M 1997 *Phys. Rev. Lett.* **78** 3201
[129] Visser D W, Ramirez A P and Subramanian M A 1997 *Phys. Rev. Lett.* **78** 3947